An Electric-Field Induced Dynamical State in Dispersions of Charged Colloidal Rods

Jan K.G. Dhont[1,2], Kyongok Kang[1]

[1] *Forschungszentrum Jülich*
Institute of Complex Systems (ICS),
Soft Condensed Matter
D-52425 Jülich, Germany.
[2] *Heinrich-Heine-Universität Düsseldorf*
Department of Physics
*D-40225 Düsseldorf, Germany.**

(Dated: February 28, 2014)

The response of concentrated dispersions of charged colloids to low-frequency electric fields is governed by field-induced inter-colloidal interactions resulting from the polarization of electric double layers and the layer of condensed ions, as well as hydrodynamic interactions through field-induced electro-osmotic flow. The phases and states that can be formed by such field-induced interactions is an essentially unexplored field of research. Experiments on concentrated suspensions of rod-like colloids (fd-virus particles), within the isotropic-nematic phase coexistence region, showed that a number of phases/states are induced, depending on the field amplitude and frequency [Soft Matter, 2010, **6**, 273]. In particular, a dynamical state is found where nematic domains form and melt on a time scale of the order of seconds. We discuss the microscopic origin of this dynamical state, which is attributed to the cyclic, electric-field induced dissociation and association of condensed ions. A semi-quantitative theory is presented for the dynamics of melting and forming of nematic domains, including a model for the field-induced dissociation/association of condensed ions. The resulting equation of motion for the orientational order parameter is solved numerically for parameters complying with the fd-virus system. A limit-cycle is found, with a cycling-time that diverges at the transition line in the field-amplitude versus frequency plane where the dynamical state first appears, in accord with experimental findings.

PACS numbers: 64.70.pv, 64.70.qj, 64.70.M-

I. INTRODUCTION

The response of concentrated dispersions of charged colloids to external electric fields has been intensively investigated for frequencies in the sub-MHz to MHz range. In two-dimensional confinement, dielectric polarization of the core of colloidal polystyrene spheres has been shown to lead to string formation [1]. Later the formation of strings and sheets has been found in three-dimensional systems (see, for example, Refs.[2–4]). These experiments are done at frequencies larger than several tens of kHz up to a MHz, where the polarization of double layers is essentially absent for the micron-sized particles that are used. Structure formation in these experiments is due to dielectric polarization of the cores of colloidal particles, resulting to dipolar-like inter-colloidal interactions. Dielectric polarization requires relatively large field amplitudes of the order of $100\,V/mm$. Spinodal-like phase separation can be induced in ferrofluids by such a strong DC electric field (larger than $750\,\mathrm{V/mm}$) [5], which can be theoretically described on the basis of a thermodynamic approach that includes the field-induced dielectric contributions to the free energy [6]. There is a large body of literature on further electric-field induced instabilities in other types of soft-matter systems, mostly in two-dimensional confinement like in thin polymer films, which is beyond the scope of the present study.

The experiments mentioned above relate to dielectric polarization at relatively high frequencies, where electric double layers are essentially unpolarized. For micron-sized colloids, polarization of the double layer (and the layer of condensed ions) ceases to occur at frequencies beyond $1-10\,kHz$. Electro-osmotic flow, however, remains active also for larger frequencies. Since this cut-off frequency scales with the radius a of the colloids and the Debye-length κ^{-1} approximately like $(a+\kappa^{-1})^{-1.5}$ [7], much higher frequencies are required to exclude double-layer polarization for smaller colloids, much smaller than a micron in diameter (for $10\,nm$ colloids, for example, the typical frequency beyond which double-layer polarization ceases to occur is of the order of several MHz).

Mesoscopically large zig-zag bands haven been found in suspensions of micron sized spherical colloids, at relatively small frequencies where electric dipoles are induced through double-layer polarization. The mechanism for the zig-zag band formation is most probably as follows. The frequency where bands appear is sufficiently large to assure a phase-lag between the field-induced double layer polarization and the external field. The dipole of a col-

*Electronic address: j.k.g.dhont@fz-juelich.de,k.kang@fz-juelich.de; URL: http://www.fz-juelich.de/ics/ics-3/DE/Home/home_node.html

loidal sphere induces a dipole within the electric double layer of a neighbouring colloid, with the corresponding additional phase-lag. There is thus a phase-lag between the dipoles directly induced by the external field and the dipoles due to mutual polarization. This phase-lag leads to a torque on each of the spheres. The rotating spheres induce a fluid flow that leads to a rotation of the doublet as a whole. In a crowded suspension, initially formed chains of spheres are destroyed beyond a critical field strength due to these rotations, after which zig-zag bands are formed. The mutual polarization need not necessarily be due to double-layer polarization, but may also be due to, for example, surface-charge polarization [8–12].

Polarization of the electric double layer (and the layer of condensed ions) is dominant for sufficiently low frequencies of the alternating electric field *and* for sufficiently low field strengths, such that dielectric polarization is essentially absent. There are quite some experimental data on anomalous birefringence in this range of low frequencies and low field strengths in suspensions that contain rod-like macromolecules. The first experiments on anomalous birefringence date back to the 1920's [13, 14], where experiments are reported on vanadium-pentoxide, gold sols, and other metallic and non-metallic colloids. In birefringence relaxation experiments on micellar systems [15, 16] and polyelectrolyte solutions [17], there is a relaxation process where the rod-like entities tend to align perpendicular to the electric field. Such an anomalous perpendicular orientation has been found under oscillatory electric fields in suspensions of fd-virus particles at very low ionic strength in a certain range of field amplitudes and frequencies [18]. In all cases the anomalous behaviour is only found for sufficiently high concentrations. The anomalous orientation is therefore most probably due to field-induced interactions through double-layer polarization and/or electro-osmotic flow, but other mechanisms like the deformation of the rod due to solvent friction and collective effects can not be excluded. The mechanisms underlying the anomalous orientation is not yet fully understood and is still under debate [19–24]. In microscopy experiments on microtubules [25], the perpendicular orientation of the longer tubules is probably due to the hydrodynamically induced bending of the rods (see in particular Fig.3d in Ref.[25]), and field-induced interactions do not play a role. Anomalous orientation is also observed in dilute suspensions of rods and spheres [26] and platelets and spheres [27], and is accompanied by a change in the turbidity of these systems [28], where the spheres are found to form complex structures around the relatively large rods and platelets. Apart from these birefringence studies, there are as yet not many experimental data on the response of concentrated colloidal dispersions to such low-frequency and low-amplitude electric fields where new phases, dynamical states and patterns are formed. In a study on suspensions of low-aspect ratio rods in the 10 kHz range, the observed structure formation is probably due to dielectric polarization of the cores of the rod-like colloids, since relatively high electric field strengths are applied [29]. In concentrated dispersions of highly charged rod-like colloids (fd-virus particles), double-layer polarization and the polarization of the layer of condensed ions, as well as hydrodynamic interactions through electro-osmotic flow, have recently been shown by the present authors to give rise to various phases, dynamical states, and non-equilibrium critical behaviour [30–32]. The fd-concentration in these experiments is within the isotropic-nematic coexistence region (without the external field). In the absence of the electric field, the system thus consists of nematic domains in coexistence with an isotropic background. In particular we found a dynamical state at low frequencies, where the nematic domains melt and form. *In this paper we aim at an explanation of the microscopic origin of this dynamical state, and to develop a semi-quantitative description for the time-dependence of melting and forming of the nematic domains.* The origin of the dynamical state is attributed to field-induced dissociation/association of condensed ions, which changes the ionic strength, and thereby the effective concentration. As will be seen, the dissociation/association of condensed ions leads to an effective concentration that oscillates around the lower isotropic-nematic binodal concentration, so that nematic domains alternatingly melt and grow. It is to be expected that the existence of dynamical states is a general feature of any suspension of highly charged an-isometric particles that form a liquid crystalline phase.

This paper is organized as follows. In the next section the phase/state diagram is briefly discussed, and the origin of the dynamical state is addressed on an intuitive level. The ingredients to describe the dynamical state are field-induced torques, polarization-charge interactions between the rods, and the field-induced dissociation of condensed ions. The torques and polarization-induced interactions are discussed in section III. The results are used as an input in the Smoluchowski equation in section IV to describe the melting and forming kinetics of nematic domains. Melting of nematic domains is analyzed on the basis of a dynamical extension of Onsager's theory for rods with a thick electric double layer, as derived from the Smoluchowski equation, including twist interactions. Growth of nematic domains from a meta-stable state is formulated in terms of an empirical equation of motion that is found in computer simulations. Another essential ingredient for the understanding of the origin of the dynamical state is the field-induced release of condensed ions. There is so far no quantitative theory that describes the frequency dependent, field-induced release of condensed ions. We therefore discuss a simple model for release of condensed ions in section V. In a numerical solution of the full set of equations of motion, it is essential to know the location of binodals and spinodals. The location of phase boundaries is determined from the above mentioned equations of motion for the orientational order parameter, as discussed in section VI. Numerical results are presented in section VII, including

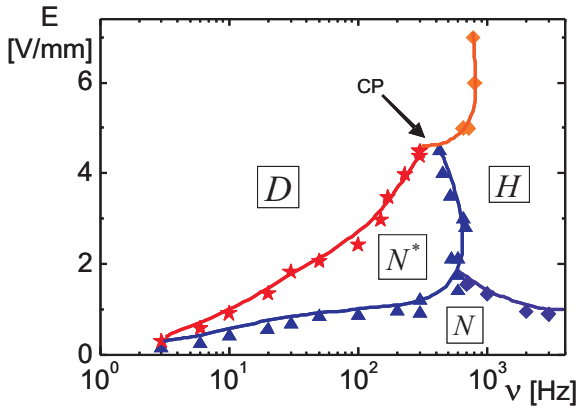

FIG. 1: The phase/state diagram in the electric-field amplitude versus frequency plane, for an fd-concentration of 2.0 mg/ml at an ionic strength of 0.16 mM. N is a phase where nematic domains coexist with an isotropic phase, $N^\star$ is a chiral nematic phase, H is a uniform homeotropic phase where the rods are aligned along the external field, and D is a dynamical state where nematic domains melt and form. "CP" indicates the non-equilibrium critical point.

a comparison with the experiments in Refs.[30–32].

II. THE STATE DIAGRAM AND THE MECHANISM THAT UNDERLIES THE DYNAMICAL STATE

In this section we describe the experimental system and the phase/state diagram [30–32], and we discuss the mechanism underlying the dynamical state.

Experiments are performed on dispersions of fd-viruses, which are dsDNA strands covered with coat proteins [35–37]. Their length is 880 nm, the thickness of the core is 6.8 nm, while the persistence length is of the order of 2500 nm. The fd-viruses are highly charged: the bare charge is $-10\,e/nm$, of which about 85% is compensated by condensed ions. These model systems for rod-like colloids have been used in the past to explore the phase behaviour of lyotropic liquid crystalline phases at relatively high ionic strength (about 5 mM or more) [33, 34, 38–41], and more recently to study the single particle dynamics within such phases in the absence of an external field [42–44]. The response of fd-virus suspensions to external electric fields is explored for fd-concentrations of 2.0 and 2.8 mg/ml, which lie within the Isotropic-Nematic (I-N) coexistence region for the low ionic strength of 0.16 mM, corresponding to a Debye length of 27 nm. Without the external field, the system thus consists of nematic domains floating in an isotropic background. Contrary to what is seen at high ionic strength, the nematic domains are now non-chiral, as the large Debye length screens core-core interactions between fd rods. The long-ranged electrostatic repulsions renders typical distances between rods sufficiently large that the helical structure of their cores does not give rise to chirality.

The experimental phase/state diagram in the electric-field versus frequency plane for a fd-concentration of $2.0\,mg/ml$ is given in Fig.1. The state where non-chiral nematic domains coexist with isotropic regions (which we referred to as the N-state), transforms to a state where the nematic domains become chiral upon increasing the field amplitude for frequencies below about 600 Hz, the $N^\star$-state in Fig.1. At relatively high frequencies (larger than 600 Hz), a uniform state exists, where the rods are aligned along the external field, perpendicular to the electrodes. We termed this phase the H-phase, where "H" stands for "homeotropic", as the rods are aligned perpendicular to the electrodes, along the field direction. At low frequencies and elevated field amplitudes a dynamical state is found, the D-state in Fig.1, where nematic domains melt and form. The time scale on which melting and forming of the nematic domains depends on the distance from the $N^\star$-to-D transition line. The melting-forming time scale diverges on approach of this transition line, that is, the dynamics of melting and forming of domains becomes arbitrary slow on approach of the $N^\star$-to-D transition line. The size of the nematic domains remains finite at the $N^\star$-to-D transition line, except on approach of the "non-equilibrium critical point", indicated by CP in Fig.1. Here, the maximum domain size during forming and subsequent melting diverges. The point indicated with CP is thus a "non-equilibrium critical point" in the sense that a time scale and a length scale diverge (critical exponents are reported in Ref.[32, 45]).

Polarization of the electric double layer and the layer of condensed ions along the long axis of a rod occurs when the frequency is sufficiently low that the ions are able to diffuse over a distance comparable to the length of a rod during the time of a cycle of the external field. An upper bound for the frequency ν where polarization is still significant is therefore estimated by $\tau_D\,\nu < 1$, where $\tau_D = D/L^2$ is the time required for ions to diffuse over the length L of the a rod (where D is the diffusion coefficient of the ions). For a typical value of the diffusion coefficient it is thus found that polarization charges are significant for frequencies below about $1\ kHz$. This frequency corresponds to the abrupt change of the phase/state diagram, above which the uniform H-phase is formed (a more quantitative estimate based on an analysis of the polarization of the layer of condensed ions will be discussed in section VII). The H-phase is therefore believed to be stabilized by "active" hydrodynamic interactions through electro-osmotic flow that is induced within the double layers and/or the layer of condensed ions. Electro-osmotic flow is active up to much higher frequencies. Hydrodynamic interactions are important when the time τ_H for a shear wave to propagate from one rod to a neighbouring rod is small as compared to the cycle time of the external field. Since $\tau_H = \rho\, l^2/\eta$ (with ρ the mass density of the solvent, l a typical distance between two rods, and η the solvent viscosity), it is found that ν should be smaller than about 1000 kHz for interactions through electro-osmotic flow to be im-

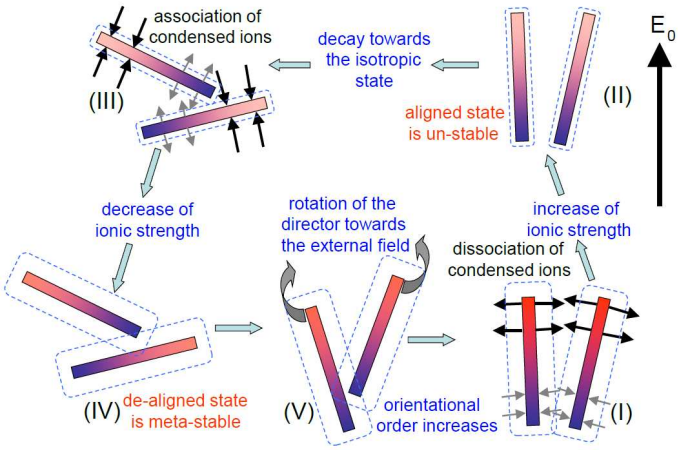

FIG. 2: The microscopic mechanism underlying the dynamical state. The various depicted stages are explained in the main text. The intensity of the red colour of the core of the rods indicates the amount of excess condensed ions, blue the depletion of condensed ions, while the dotted lines around the cores indicate the extent of the electric double layer. Typical cycling times are $2\,s$ away from the transition line and diverges on approach of the transition line.

portant.

In an attempt to develop an understanding of the microscopic origin of the stabilization mechanisms of the various phases and states in the diagram in Fig.1, one can thus distinguish two separate regimes. For frequencies larger than about 1 kHz, a theory could be developed that neglects interactions through field-induced polarization charges, and only accounts for electro-osmotic flow. For frequencies below 1 kHz, interactions through polarization charges are dominant, so that a theory could be developed that is based on field-induced interactions through polarization charges. In this paper we consider the latter, low-frequency regime. In particular *it is the aim of the present study to explain the microscopic origin of the dynamical state D, where nematic domains melt and form.*

Based on the theory developed in the present paper, the existence of the dynamical state can only be explained through field-induced dissociation/association of condensed ions. Fd-virus particles carry many condensed ions, where about 85 % of the bare charge of 8.800 elementary charges is compensated by condensed ions. As will be seen later in section VII, where explicit numerical results will be discussed, this amount of condensed is sufficient to make the following mechanism underlying the dynamical state feasible. A nematic domain will be oriented towards the direction of the electric field by single particle torques. The layer of condensed ions rods will be significantly polarized once the rods are aligned along the field (see (I) in Fig.2). Condensed ions will be repelled into the solvent when there is an excess amount of condensed ions (indicated by red in Fig.2), and ions will be drawn from the solvent towards the layer of condensed ions when there is a shortage of condensed ions due to polarization (indicated by blue). The resulting net release of condensed ions leads after some time to an increase of the bulk ionic strength. This increase of the bulk ionic strength leads to a decrease of the extent of the electric double layers (see Fig.2(II)). Dotted blue lines around the cores are used in Fig.2 to indicate the extent of the double layers. In (II) the double-layer thickness is smaller than in (I) due to the release of condensed ions. The effective concentration therefore decreases. When the effective concentration becomes smaller than the lower binodal concentration, the nematic domains become unstable and will melt, so that the degree of orientational order decreases (as shown in (III)). Due to decreasing degree of alignment along the field direction, re-condensation will occur (see (III)). Re-condensation leads to a decrease of bulk ionic strength, so that the double-layer thickness increases (see (IV)). The effective volume fraction increases accordingly, and the system re-enters the two-phase isotropic-nematic coexistence region (see (IV)). Orientational order now increases, and at the same time the domains that form are orientated along the electric-field direction due to the torques with which the electric field acts on single rods (see (V)). The degree of polarization of the condensed layer increases as the domains align along the field direction, leading to release of condensed ions (see again (I)), after which the entire cycle repeats itself.

The location of the $N^\star - D$ phase boundary in Fig.1 (in red) is thus determined by the amount of dissociated condensed ions that is needed to bring the system to an effective rod-concentration equal to the lower isotropic-nematic binodal concentration. Clearly there is a minimum electric field amplitude necessary to give rise to sufficient release of condensed-ion. This minimum value for the field amplitude increases with increasing frequency, since larger frequencies lead to a diminished polarization, and thereby to a decrease of the number of released ions. This explains the larger field amplitude needed to induce the D-state with increasing frequency. The transition from the non-chiral N-phase to the chiral $N^\star$-phase can also be understood in terms of release of condensed ions. The ionic strength at sufficiently large field amplitudes is increased through the release of condensed ions, which renders the nematic chiral, just as for the equilibrium nematic without a field at higher ionic strengths, which is due to the helicity of the DNA strand that constitutes the fd-virus particles [38, 46–48]. The field amplitude within the $N^\star$-phase is not yet large enough to render the nematic domains unstable, but is sufficiently large to transform the non-chiral nematic to a chiral nematic.

Spatial variations in the dielectric constant can give rise to electric-field induced instabilities [5, 6, 9, 10]. For the present experiments, however, the field strengths (up to about $5\,V/mm$) are too low to induced sufficient dielectric polarization, and the concentration of fd-virus particles is very low (the volume fraction is about 0.002), which most probably leads to a minor effect due to di-

electric polarization even for much higher field strengths. In addition, the type of instability described here, where quasi time-periodic patterns are seen, is of a quite different nature as compared to the spinodal-like demixing induced by spatial variations in the dielectric constant.

III. FIELD-INDUCED TORQUES AND POLARIZATION-CHARGE INTERACTIONS

In this section we describe the frequency dependent torques and rod-rod pair interactions due to the electric field induced polarization charges within the layer of condensed ions. The assumption here is that the majority of ions is accumulated around the core of the rods, so that the contributions due to polarization of the diffuse double layer is of minor importance. It is important to have a (semi-) quantitative prediction of the frequency dependence of polarization, in order to understand the frequency dependence of the location of transition lines, as well as the D-state dynamics. In the first subsection the results from the theory for polarization as described in Ref.[49] will be summarized. On the basis of this theory the torque on a rod due to the external field is calculated in subsection III B, and the pair-interaction potential due to polarization charges is calculated in subsection III C. The torque and pair-interaction potential will be used as an input to the Smoluchowski equation in order to predict the dynamics of the orientational order parameter.

A. Polarization of the layer of condensed ions

There is a large body of work, sometimes dating many decades back, where the various polarization mechanisms of colloidal particles have been addressed. The frequency-dependent polarization of colloids can be formulated in terms of an effective dielectric constant, which depends on the bare dielectric constants and the conductivities of the solvent and the colloid. This early approach is known as the Maxwell-Wagner theory [51], which ignores the existence of an electric double layer containing mobile ions. In case of a thin electric double layer, the polarization of the double layer can be accounted for within such a Maxwell-Wagner approach as an additional contribution to the surface conductivity, as first suggested by O'Konski [50]. The double-layer polarization in this case does not lead to an additional relaxation time of the charge distribution, as it simply changes the value of the surface conductivity. The surface conductivity due to the presence of a thin double layer can be expressed in terms of the surface potential and the diffusion coefficient of the ions, assuming that the curvature of the colloidal-core surface is much larger than the thickness of the double layer [52, 53]. The Maxwell-Wagner approach, originally formulated for spherical colloids, can also be used to approximately predict the polarization of rod-like colloids [54, 55]. These theories are limited to thin double layers. The presence of thick double layers leads to an additional polarization relaxation process at lower frequencies, and can not be accounted for through an effective surface conductivity. The mathematics involved in the analysis of thick double layers is much more complicated as compared to that for thin double layers. Besides a number of theories where specific assumptions need to be made to arrive at analytical results, and there are numerical solutions of the standard electro-kinetic equations in which such approximations are not necessary, and which in particular allow large surface potentials (see, for example, Refs.[56–63], and references therein). A recently developed approach based on the Smoluchowski equation in mode-coupling approximation, where the small ions are treated as Brownian particles of finite size and which includes hydrodynamic coupling between the small ions and the colloidal particle, allows for the (partly numerical) calculation of transport properties of charged colloids [64, 65]. The polarization of the layer of condensed ions in a DC electric field has been discussed both for low and high field amplitudes by Manning [66, 69]. The above cited work is just a small selection from the large body of work that has been published in this area. For a more extensive overview we refer to the book of Russel [67] and the series of books by Lyklema [68] (in particular Volume II).

As mentioned in section II, about 85 % of the charged groups, chemically bound to the surface of an fd-virus particle, is compensated by condensed ions. Only 15 % of the ions reside within the diffuse double layer. The calculations concerning the dynamical state will therefore be based on the frequency-dependent solution of the standard kinetic equations applied to a mobile layer of ions, where the ions are constrained to move along the surface of a cylindrical rod [49]. In this subsection we will summarize this relatively simple model, and state the results for response functions for the polarization charge. Manning [69] developed a similar approach for a discrete bare-charge distribution, which is a more realistic description for polyelectrolytes, and obtains very similar results for the polarization as in Ref.[49] for a continuous bare-charge distribution on a cylindrical colloid. The ions in solution respond to the electric field that is produced by the inhomogeneous charge distribution of the condensed ions. The inhomogeneous surface charge distribution gives rise to an inhomogeneous diffuse double layer, with a local charge density that is opposite in sign to the local surface charge density of the mobile condensed ions. The frequency of the external field is assumed to be sufficiently small, such that this non-homogeneous diffuse double layer is in instantaneous equilibrium with the condensate. The frequency ν of the external field is therefore assumed to obey the following criterion,

$$\frac{\nu}{2\,D_0\,\kappa^2} \ll 1\,,$$

where D_0 is the diffusion coefficient of ions in solution

and κ is the inverse Debye screening length,

$$\kappa \;=\; \sqrt{\frac{2\,\beta\,e^2\,c_0}{\epsilon}}\;, \qquad (1)$$

with $\beta = 1/k_BT$ (with k_B Boltzmann's constant and T the temperature), $e > 0$ is the elementary charge, c_0 is the concentration of ions in solution outside the double layer, and ϵ is the static dielectric constant of the solvent. It is assumed here that only mono-valent ions are present.

We consider thin and long rods, such that the aspect ratio,

$$p \;=\; \frac{L}{2a}\;,$$

is a large number (with a the radius of the core, and L it's length). The polarization surface charge density for rods oriented parallel to the external field is typically a factor p larger than the charge induced in case of perpendicular orientation. The perpendicularly induced charge density is therefore neglected, and only polarization along the long axis of the rod is considered.

The external electric field that is considered is spatially uniform and sinusoidally varying with time,

$$\mathbf{E}(t) \;=\; \mathbf{E}_0\,\cos\{\omega\,t\}\;,$$

where $\nu = \omega/2\,\pi$ is the frequency of the field. Without loss of generality, the field amplitude $\mathbf{E}_0$ is taken along the z-direction.

The total concentration c of condensed ions is the sum of the uniform surface concentration $\bar{c}$ of mobile ions that exists in the absence of the external field, and a non-uniform contribution Δc to the concentration of condensed ions that is induced by the external electric field,

$$c \;=\; \bar{c} + \Delta c\;.$$

In Ref.[49] the total charge density is taken zero in case of the unpolarized rod. Here we assume the more realistic situation where the rod still carries a net surface charge density σ_0 when the rod is not polarized, so that (again for mono-valent ions),

$$\sigma \;=\; \sigma_0 + \sigma_P \quad,\quad \sigma_P \;=\; e\,\Delta c\;,$$

where σ_P is the surface charge density resulting from polarization. The surface charge density σ_P that results from polarization of the condensate can be written in terms of the in-phase $R^{'}$ and out-phase $R^{''}$ response functions [49],

$$\sigma_P(\mathbf{r}\,|\,\omega,t) \;=\; R^{'}_{c,\,\|}(\mathbf{r}\,|\,\omega)\,\cos\{\omega t\} + R^{''}_{c,\,\|}(\mathbf{r}\,|\,\omega)\,\sin\{\omega t\}\;.$$

The subscript "c" is used to indicate that these response functions relate to polarization of the layer of condensed ions, while the subscript " $\|$ " refers to the parallel orientation that will be considered in the present analysis where perpendicular polarization is neglected. The potential can be similarly written in terms of in-phase and out-phase response functions.

The frequency where the out-phase response functions become significantly non-zero for polarization along the rod's long axis is set by the dimensionless frequency,

$$\Lambda_{\|} \;=\; \frac{\omega\,L^2}{4\,D^{\rm eff}}\;,$$

with $D^{\rm eff}$ the effective diffusion coefficient of the condensed ions,

$$D^{\rm eff} \;=\; D\,\left[\,1 + 2\,\kappa_c\,a\,\mathcal{K}(\kappa\,a)\,\right]\;, \qquad (2)$$

where D is the bare diffusion coefficient of condensed ions, and,

$$\kappa_c \;=\; \frac{e^2\,\beta\,\bar{c}}{2\,\epsilon} \;=\; 2\,\pi\,l_B\,\bar{c} \;=\; 2\,\frac{l_B}{d\,L}\,N_c\;, \qquad (3)$$

is the inverse "condensate length", l_B is the Bjerrum length, and N_c is the total number of condensed ions on a rod. Furthermore,

$$\mathcal{K}(\kappa\,a) \;\equiv\; \frac{1}{2\,\pi}\,\int_0^{2\pi} d\varphi\;K_0\Big(\kappa\,a\sqrt{2\,(1-\cos\varphi)}\Big)\;, \qquad (4)$$

with K_0 the modified Bessel function of the second kind of zeroth order. This function is plotted in Fig.3a. For sufficiently thick double layers where $\kappa\,a \lesssim 0.3-0.4$, this function is to a good approximation equal to $-\ln\{\kappa\,a\}$ (see the dashed-dotted line in Fig.3a).

The effective diffusion coefficient in eq.(2) is larger than the bare diffusion coefficient D of condensed ions due to their repulsive interactions. An inhomogeneous condensate distribution, without an external field, relaxes to the homogeneous distribution faster as a result of the repulsive inter-ion interactions. The bare diffusion coefficient D of the condensed ions is generally smaller than that of ions in solution, since the condensed ions experience an additional friction with the core of the rod.

The in-phase and out-phase response functions for parallel orientation are given by,

$$\begin{pmatrix} R^{'}_{c,\,\|}(z\,|\,\omega) \\ R^{''}_{c,\,\|}(z\,|\,\omega) \end{pmatrix} \;=\; \frac{\epsilon\,\kappa_c\,L\,E_{0,\,\|}}{1 + 2\,\kappa_c\,a\,\mathcal{K}(\kappa\,a)} \qquad (5)$$
$$\times \begin{pmatrix} F^{(-)}(\Omega) & F^{(+)}(\Omega) \\ F^{(+)}(\Omega) & -F^{(-)}(\Omega) \end{pmatrix} \cdot \begin{pmatrix} \cos\{2\,\Omega\,z/L\} & \sinh\{2\,\Omega\,z/L\} \\ \sin\{2\,\Omega\,z/L\} & \cosh\{2\,\Omega\,z/L\} \end{pmatrix},$$

where $z \in [-\frac{1}{2}L, \frac{1}{2}L]$ is the coordinate along the long axis of the rod, and $E_{0,\|}$ is the component of the external field along the long axis of the rod. Furthermore the quantity,

$$\Omega \;=\; \big(\Lambda_{\|}/2\big)^{1/2}\;, \qquad (6)$$

is introduced for convenience, and,

$$F^{(\pm)}(\Omega) \;=\; \frac{1}{\Omega}\,\frac{\cos\{\Omega\}\,\cosh\{\Omega\} \pm \sin\{\Omega\}\,\sinh\{\Omega\}}{\cos\{2\,\Omega\} + \cosh\{2\,\Omega\}}\;.$$

It should be noted that the contour variable z varies in the direction of the electric field, that is, with increasing z the corresponding location on the core changes in the direction of the external field.

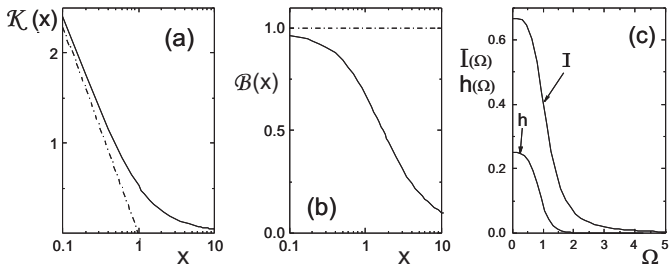

FIG. 3: (a) The function $\mathcal{K}(x=\kappa a)$ in eq.(4). The solid line is obtained by numerical integration, and the dashed-dotted line is the asymptotic value $-\ln\{\kappa\, a\}$ of $\mathcal{K}$ for small $\kappa\, a$. (b) The function $\mathcal{B}$ defined in eq.(10). The asymptotic form of this function is unity. (c) The functions I and h, defined in eqs.(9) and (40), respectively. The function I describes the frequency dependence of single particle torques, while the function h characterizes the interactions strength between polarization charges. The dimensionless frequency Ω is defined in eq.(6).

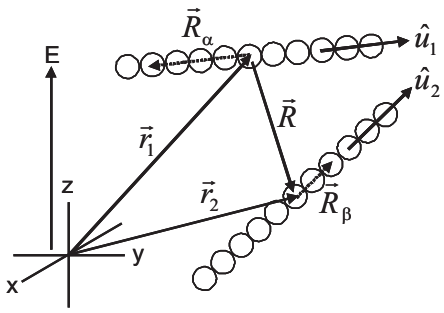

FIG. 4: The bead model for the calculation of the interaction potential between two rods, which is valid in case $\kappa\, a \lesssim 1$. The coordinates $\mathbf{r}_1$ and $\mathbf{r}_2$ are the positions of the centers of the two rods, while the unit vectors $\hat{\mathbf{u}}_1$ and $\hat{\mathbf{u}}_2$ specify their orientation. The positions $\mathbf{R}_\alpha$ of bead α of rod number 1 and $\mathbf{R}_\beta$ of bead β within rod 2 are taken with respect to the centers of the rods (for the specific example shown here, $\alpha=-4$ and $\beta=2$).

B. The torque on a rod

The electric field exerts a torque on each rod that tends to align them along the direction of the field. In Ref.[49] we derived an expression for the torque due to polarization of the layer of condensed ions, both due to polarization parallel and perpendicular to the long axis of a rod. It is shown there that the torque due to polarization in the directions perpendicular to the rod's long axis is a factor p^{-2} smaller than the torque due to polarization parallel to the rod. The torque due to perpendicular polarization can therefore be neglected for long and thin rods. The parallel-polarization torque, averaged over a cycle of the external field, is equal to,

$$\mathbf{T}_{\parallel}(\hat{\mathbf{u}},t) \;=\; \frac{\pi}{8}\, L^3\, (\hat{\mathbf{u}}\times\mathbf{E}_0)\, (\hat{\mathbf{u}}\cdot\mathbf{E}_0)\, \epsilon\, F_1(\Omega)\, F_3\;. \quad (7)$$

Here,

$$\begin{aligned} F_1(\Omega) \;&=\; V(\kappa_c a)\,\left[\, W(\kappa_c a,\kappa a)+1\,\right]\, I(\Omega)\;,\\ F_3 \;&=\; 2\left[\,1+\kappa_c\, a\,\mathcal{B}(\kappa\, a)\right]^2 - \kappa_c\, a\left[\,1+\kappa_c\, a\,\mathcal{B}(\kappa\, a)\,\right]\;, \end{aligned} \quad (8)$$

where, V, W and I stand for,

$$\begin{aligned} V(\kappa_c a) \;&=\; \frac{\kappa_c\, a}{\left(\,1+\kappa_c\, a\,\mathcal{B}(\kappa\, a)\right)^2}\;,\\ W(\kappa_c a,\kappa a) \;&=\; -\,\frac{2\,\kappa_c\, a\,\mathcal{K}(\kappa\, a)}{1+2\,\kappa_c\, a\,\mathcal{K}(\kappa\, a)}\;,\\ I(\Omega) \;&=\; \frac{1}{2\,\Omega^3}\,\frac{\sinh\{2\,\Omega\}-\sin\{2\,\Omega\}}{\cosh\{2\,\Omega\}+\cos\{2\,\Omega\}}\;, \end{aligned} \quad (9)$$

and where $\mathcal{K}$ is the function defined in eq.(4), while,

$$\mathcal{B}(\kappa\, a) \equiv \frac{1}{\pi}\int_0^{2\,\pi} d\varphi\, \cos\{\varphi\}\, K_0\Big(\kappa\, a\,\sqrt{2(1-\cos\varphi)}\,\Big)\;, \quad (10)$$

which function is plotted in Fig.3b. The asymptotic value of $\mathcal{B}$ for small values of κa is unity. The frequency dependent function I in eq.(9) is plotted in Fig.3c.

C. Interactions between two rods

When the Debye length is larger than the core diameter d, the interaction potential between two rods may be approximated by pair-wise additive interactions between spherical beads that constitute the two rods (as sketched in Fig.4). The charge distribution within the diffuse double layer of a given bead is essentially unaffected by the presence of relatively small volume that is occupied by neighbouring beads [70]. The double layer structure of a rod can thus be represented as a sum of spherical double layers of beads with radius a. The positions of the beads on rod number 1 are written as $\mathbf{r}_1+\mathbf{R}_\alpha$, where $\mathbf{r}_1$ is the center of the rod, and $\mathbf{R}_\alpha$ is the position of the center of a bead relative to the center of the rod, as sketched in Fig.4. The bead-index number α ranges from 0 for the bead at the center of the rod, to $\pm N$ for the beads at the ends of the rod. The number of beads is thus equal to $2N+1$, and the aspect ratio is equal to $p=1/(2N+1)$. The orientation of rod 1 is specified by the unit vector $\hat{\mathbf{u}}_1$ along the long axis of the rod (see Fig.4). The relative bead coordinates can thus be expressed as $\mathbf{R}_\alpha=\alpha\, d\,\hat{\mathbf{u}}_1$. Similar coordinates are introduced for rod number 2. In the following we will use the bead-number indices α and β for rod 1 and 2, respectively.

The charge Q_α^{total} on each bead α is the sum of the charge $\bar{Q}$ that would be present without the external field, and the charge Q_α due to polarization,

$$Q_\alpha^{total} \;=\; \bar{Q}+Q_\alpha\;.$$

For sufficiently small net charge densities and sufficiently thick double layers, the instantaneous interaction potential between two beads is equal to the Debye-Hückel po-

tential $V_Q(\alpha,\,\beta)$,

$$V_Q(\alpha,\,\beta) \;=\; \frac{\exp\{\kappa\, d\}}{4\,\pi\,\epsilon\;(\,1+\kappa\, a\,)^2}\;\left[\,Q_\alpha+\bar{Q}\,\right]\;\left[\,Q_\beta+\bar{Q}\,\right] \times\frac{exp\,\{-\kappa\,|\,\mathbf{R}+d\;(\,\beta\,\hat{\mathbf{u}}_2-\alpha\,\hat{\mathbf{u}}_1)\,|\}}{|\,\mathbf{R}+d\;(\,\beta\,\hat{\mathbf{u}}_2-\alpha\,\hat{\mathbf{u}}_1)\,|}\;,$$

where $\mathbf{R}=\mathbf{r}_2-\mathbf{r}_1$ is the distance between the centers of the two rods. The total potential between the two rods is the pair-wise sum over all beads,

$$V_Q(\mathbf{R},\hat{\mathbf{u}}_1,\hat{\mathbf{u}}_2) \;=\; \sum_{\alpha,\beta=-N}^{N} V_Q(\alpha,\beta)\;. \tag{11}$$

The index Q is used to indicate that this is the potential due to charge interactions. The bead-charges due to polarization can be found from,

$$Q_\alpha \;\equiv\; Q(z=\alpha\,d) \;=\; 4\,\pi\,a^2 \times\Big[R^{'}_{c,\,\parallel}(z=\alpha\,d|\,\omega)\;\cos\{\omega\,t\}+R^{''}_{c,\,\parallel}(z=\alpha\,d|\,\omega)\;\sin\{\omega\,t\}\Big]\,, \tag{12}$$

where the response functions are given in eq.(5). Rewriting the double summation in eq.(11) as a double contour integral, and substitution of eqs.(11,12) leads to a quite complicated expression for the potential, which is not amenable for further analytical evaluation. Due to the fact that the bead interactions are screened over the Debye length κ^{-1}, which is very small as compared to the length scale on which the polarization surface-charge density significantly changes along the contour of the rod, an accurate approximation can be made that leads to a relatively simple expression for the potential. When the degree of alignment of the rods is not too high, there are only a few beads on the two rods which are within a distance of a few times the Debye length. All other beads are further apart, and do essentially not contribute to the rod-rod interaction potential. These few interacting beads on each of the two rods have essentially the same charges. Let α_0 and β_0 denote the bead index number on rod 1 and 2, respectively, for which the distance between the two beads is minimal for a given $\mathbf{R}$, $\hat{\mathbf{u}}_1$ and $\hat{\mathbf{u}}_2$. The potential (11) can then be approximated as,

$$V_Q(\mathbf{R},\hat{\mathbf{u}}_1,\hat{\mathbf{u}}_2) \;=\; \mathcal{N}\,V_Q(\alpha_0,\beta_0)\;, \tag{13}$$

where $\mathcal{N}$ is the number of interacting beads. For perpendicular orientation of the two rods, the number of beads that interact is $\sim 1/(\kappa\,a)^2$, while this number increases like $\sim 1/\,|\,\hat{\mathbf{u}}_1\times\hat{\mathbf{u}}_2\,|$ for non-perpendicular orientations. Hence,

$$\mathcal{N} \;=\; \frac{1}{(\kappa\,a)^2\;|\,\hat{\mathbf{u}}_1\times\hat{\mathbf{u}}_2\,|}\quad,\quad \kappa\,a\lesssim 1\;. \tag{14}$$

This estimate is to be taken seriously only for orientations where the rods are not parallel, since in this case the approximation (13) fails. We will assume that the rods are sufficiently long and thin, and that the orientational order parameter is sufficiently low, that contributions from semi-parallel orientations where $|\,\hat{\mathbf{u}}_1\times\hat{\mathbf{u}}_2\,|\lesssim 1/p=d/L\ll 1$ can be neglected.

The distance $\mathbf{\Delta}$ between two beads α on rod 1 and β on rod 2 is equal to,

$$\mathbf{\Delta} \;=\; \mathbf{R}+\beta\,d\,\hat{\mathbf{u}}_2-\alpha\,d\,\hat{\mathbf{u}}_1\;. \tag{15}$$

For very long and thin rods, the probability for an tip-body or tip-tip interaction is very small, except in phases like a smectic phase or a columnar phase. Here we shall only consider isotropic and nematic phases, where body-body interactions determine the behaviour of concentrated suspensions. Hence, we assume that the two beads with the minimum distance are located within the body of both rods. In that case, the minimal distance $\mathbf{\Delta}_0$ is of the form,

$$\mathbf{\Delta}_0 \;=\; C\,\hat{\mathbf{v}}\;, \tag{16}$$

where the prefactor C depends on $\mathbf{R}$, $\hat{\mathbf{u}}_1$ and $\hat{\mathbf{u}}_2$, and,

$$\hat{\mathbf{v}} \;=\; \frac{\hat{\mathbf{u}}_1\times\hat{\mathbf{u}}_2}{|\,\hat{\mathbf{u}}_1\times\hat{\mathbf{u}}_2\,|}\;, \tag{17}$$

is the unit vector perpendicular to both $\hat{\mathbf{u}}_1$ and $\hat{\mathbf{u}}_2$. The prefactor is immediately found from eqs.(15-17),

$$C \;=\; (\mathbf{R}\cdot\hat{\mathbf{v}})\;,$$

while the bead index number α_0 is found to be equal to,

$$\alpha_0 \;=\; \frac{1}{d}\,\frac{\mathbf{R}\cdot\hat{\mathbf{u}}_1-(\mathbf{R}\cdot\hat{\mathbf{u}}_2)\;(\hat{\mathbf{u}}_1\cdot\hat{\mathbf{u}}_2)}{|\,\hat{\mathbf{u}}_1\times\hat{\mathbf{u}}_2\,|^2}\;, \tag{18}$$

and similarly,

$$\beta_0 \;=\; \frac{1}{d}\,\frac{-\mathbf{R}\cdot\hat{\mathbf{u}}_2+(\mathbf{R}\cdot\hat{\mathbf{u}}_1)\;(\hat{\mathbf{u}}_1\cdot\hat{\mathbf{u}}_2)}{|\,\hat{\mathbf{u}}_1\times\hat{\mathbf{u}}_2\,|^2}\;. \tag{19}$$

Putting all the above results together, the pair-interaction potential can be written as a sum of a contribution V_{EE} due to interactions between polarization charges, the potential $V_{\bar{Q}\bar{Q}}$ due to interactions in the absence of the electric field, and $V_{E\bar{Q}}$ due to interactions between charged beads in the absence of the field and charges due to polarization,

$$V_Q(\mathbf{R},\hat{\mathbf{u}}_1,\hat{\mathbf{u}}_1) \;= V_{EE}(\mathbf{R},\hat{\mathbf{u}}_1,\hat{\mathbf{u}}_1)+V_{\bar{Q}\bar{Q}}(\mathbf{R},\hat{\mathbf{u}}_1,\hat{\mathbf{u}}_1)+V_{E\bar{Q}}(\mathbf{R},\hat{\mathbf{u}}_1,\hat{\mathbf{u}}_1)\,. \tag{20}$$

The interaction potential V_{EE} is found to be given by,

$$\beta\,V_{EE}(\mathbf{R},\hat{\mathbf{u}}_1,\hat{\mathbf{u}}_2) \;=\; K_E\;\mathcal{E}_0^2\;\frac{\hat{u}_{1,\,z}\,\hat{u}_{2,\,z}}{|\,\hat{\mathbf{u}}_1\;\times\;\hat{\mathbf{u}}_2\,|} \times\frac{\exp\{-\kappa\;|\,\mathbf{R}\cdot(\hat{\mathbf{u}}_1\times\hat{\mathbf{u}}_2)|\;/\;|\,\hat{\mathbf{u}}_1\times\hat{\mathbf{u}}_2\,|\}}{\kappa\;|\,\mathbf{R}\cdot(\hat{\mathbf{u}}_1\times\hat{\mathbf{u}}_2)|\;/\;|\,\hat{\mathbf{u}}_1\times\hat{\mathbf{u}}_2\,|} \times[\,G(S_1)\;\cos\{\omega\,t\}+H(S_1)\;\sin\{\omega\,t\}\,] \times[\,G(S_2)\;\cos\{\omega\,t\}+H(S_2)\;\sin\{\omega\,t\}\,]\;, \tag{21}$$

where the dimensionless external field is introduced,

$$\mathcal{E}_0 \;=\; \beta\, e\, L\, E_0 \;,$$

which is the energy required to displace an ion over the rod length against the electric field in units of the thermal energy, and where,

$$\begin{aligned} K_E \;&=\; \frac{(\kappa_c/\kappa)^2\,\exp\{\kappa\, d\}}{4\,(1+\kappa\, a)^2\,(1+2\,k_c\, a\,\mathcal{K}(\kappa\, a))^2}\,\frac{\kappa\, d^2}{l_B} \\ &=\; \frac{\exp\{\kappa\, d\}}{(1+\kappa\, a)^2\,(1+2\,k_c\, a\,\mathcal{K}(\kappa\, a))^2}\,\frac{l_B}{\kappa\, L^2}\,N_c^2\;, \end{aligned} \tag{22}$$

is a dimensionless constant, where again N_c is the number of condensed ions per rod. Furthermore,

$$\begin{aligned} G(S) \;&=\; F^{(-)}(\Omega)\,\cos\{S\}\,\sinh\{S\} \\ &\qquad +F^{(+)}(\Omega)\,\sin\{S\}\,\cosh\{S\}\;, \\ H(S) \;&=\; F^{(+)}(\Omega)\,\cos\{S\}\,\sinh\{S\} \\ &\qquad -F^{(-)}(\Omega)\,\sin\{S\}\,\cosh\{S\}\;, \end{aligned}$$

with S either equal to S_1 or S_2,

$$\begin{aligned} S_1 \;&=\; \frac{2\,\Omega}{L}\,\frac{\mathbf{R}\cdot\hat{\mathbf{u}}_1-(\mathbf{R}\cdot\hat{\mathbf{u}}_2)\,(\hat{\mathbf{u}}_1\cdot\hat{\mathbf{u}}_2)}{|\,\hat{\mathbf{u}}_1\times\hat{\mathbf{u}}_2\,|^2}\;, \\ S_2 \;&=\; -\,\frac{2\,\Omega}{L}\,\frac{\mathbf{R}\cdot\hat{\mathbf{u}}_2-(\mathbf{R}\cdot\hat{\mathbf{u}}_1)\,(\hat{\mathbf{u}}_1\cdot\hat{\mathbf{u}}_2)}{|\,\hat{\mathbf{u}}_1\times\hat{\mathbf{u}}_2\,|^2}\;. \end{aligned} \tag{23}$$

The potential $V_{\bar{Q}\bar{Q}}$ is equal to,

$$\begin{aligned} \beta\, V_{\bar{Q}\bar{Q}}(\mathbf{R},\hat{\mathbf{u}}_1,\hat{\mathbf{u}}_2) \;&=\; K_Q\,\frac{1}{|\,\hat{\mathbf{u}}_1\,\times\,\hat{\mathbf{u}}_2\,|} \\ &\times\frac{\exp\{-\kappa\;|\mathbf{R}\cdot(\hat{\mathbf{u}}_1\times\hat{\mathbf{u}}_2)|\;/\;|\,\hat{\mathbf{u}}_1\times\hat{\mathbf{u}}_2\,|\}}{\kappa\;|\mathbf{R}\cdot(\hat{\mathbf{u}}_1\times\hat{\mathbf{u}}_2)|\;/\;|\,\hat{\mathbf{u}}_1\times\hat{\mathbf{u}}_2\,|}\;, \end{aligned} \tag{24}$$

with,

$$\begin{aligned} K_Q \;&=\; \frac{4\,Z^2\,\exp\{\kappa\, d\}}{(1+\kappa\, a)^2}\,\frac{l_B}{\kappa\, L^2} \\ &=\; \frac{4\,\exp\{\kappa\, d\}}{(1+\kappa\, a)^2}\,\frac{l_B}{\kappa\, L^2}\,(\,N_0-N_{c,\,0}\,)^2\;, \end{aligned} \tag{25}$$

with Z the valency of the entire rod, that is, the total excess number of elementary charges of the unpolarized rod, N_0 is the number of immobile charges on the surface of the rod and $N_{c,0}$ is the number of condensed ions in the absence of the electric field. Note that $Z\,e\,(N_0-N_{c,0})$ is the total charge of the rod. We will not specify the potential $V_{E\bar{Q}}$ for reasons given below. The validity of the above expressions is limited to those combinations of relative positions and orientations where α_0 and β_0 in eqs.(18,19) are in $[-p/2,p/2]$, where as before, p is the aspect ratio. When for given values of the position and orientations α_0 and/or β_0 are outside this range, the potential is understood to be zero by construction.

For sufficiently large frequencies the configuration of rods does not change during a cycle of the external field. For fd virus this is the case for frequencies larger than a few tens of Hz. We can therefore time-average the potential V_Q over one cycle of the external field, which finally leads to (with the overbar denoting averaging over a cycle of the external field),

$$\bar{V}_Q(\mathbf{R},\hat{\mathbf{u}}_1,\hat{\mathbf{u}}_1) \;=\; \bar{V}_{EE}(\mathbf{R},\hat{\mathbf{u}}_1,\hat{\mathbf{u}}_1)+V_{\bar{Q}\bar{Q}}(\mathbf{R},\hat{\mathbf{u}}_1,\hat{\mathbf{u}}_1)\;,$$

where,

$$\begin{aligned} &\beta\,\bar{V}_{EE}(\mathbf{R},\hat{\mathbf{u}}_1,\hat{\mathbf{u}}_2) \;= \\ &\tfrac{1}{2}\,\{\,G(S_1)\,G(S_2)+H(S_1)\,H(S_2)\,\}\,K_E\,\mathcal{E}_0^2\,\frac{\hat{u}_{1,\,z}\,\hat{u}_{2,\,z}}{|\,\hat{\mathbf{u}}_1\,\times\,\hat{\mathbf{u}}_2\,|} \\ &\qquad\times\frac{\exp\{-\kappa\;|\mathbf{R}\cdot(\hat{\mathbf{u}}_1\times\hat{\mathbf{u}}_2)|\;/\;|\,\hat{\mathbf{u}}_1\times\hat{\mathbf{u}}_2\,|\}}{\kappa\;|\mathbf{R}\cdot(\hat{\mathbf{u}}_1\times\hat{\mathbf{u}}_2)|\;/\;|\,\hat{\mathbf{u}}_1\times\hat{\mathbf{u}}_2\,|}\;, \end{aligned} \tag{26}$$

while $V_{\bar{Q}\bar{Q}}$ is not affected by averaging, and $\bar{V}_{E\bar{Q}}=0$ (this potential is $\sim\;[G(S)\,\cos\{\omega\, t\}+H(S)\,\sin\{\omega\, t\}]$, which vanishes upon averaging). The important implication of the slow response of the configuration of rods is that configurational probability functions are essentially equal to those in equilibrium, with the potential between the rods equal to $\bar{V}_Q$. This is essential for the derivation of the equation of motion for the orientational order parameter tensor.

IV. MELTING AND FORMING KINETICS OF NEMATIC DOMAINS

The larger part of this section is concerned with the kinetics of melting of nematic domains when the ionic strength is sufficiently large that the nematic state is unstable, that is, when the effective concentration is lower than the lower binodal concentration. Equations of motion for the orientational order parameter are derived, which not only describe the kinetics of melting, but are also essential to determine the location of isotropic-nematic phase boundaries. The kinetics of formation of domains is described on the basis of a simple, empirical equation of motion that is found in computer simulations. Since the nematic domains are large compared to the size of single rods, and the interfaces between nematic domains and isotropic regions seem quite diffuse (as seen experimentally), the kinetics will be described on the basis of equations of motion for a homogeneous system.

A. Melting kinetics

Starting point for the analysis of melting kinetics is the Smoluchowski equation for an assembly of N uniaxial, stiff rods, which is the fundamental equation of motion for the probability density function (pdf) $P(\mathbf{r}_1,\cdots,\mathbf{r}_N,\hat{\mathbf{u}}_1,\cdots,\hat{\mathbf{u}}_N,t)$ of all the positions $\mathbf{r}_j$ and orientations $\hat{\mathbf{u}}_j$ of the rods (with particle number index

$j = 1, 2, \cdots, N$) in the overdamped limit. The Smoluchowski equation for very long and thin rods reads,

$$\frac{\partial P}{\partial t} = \sum_{j=1}^{N} \left[\tfrac{3}{4} D_t \nabla_j \cdot \left[\hat{\mathbf{I}} + \hat{\mathbf{u}}_j \hat{\mathbf{u}}_j \right] \cdot \left\{ \nabla_j P + \beta P \left[\nabla_j \Psi - \mathbf{F}_j^{(1)} \right] \right\} + D_r \hat{\mathcal{R}}_j \cdot \left\{ \hat{\mathcal{R}}_j P + \beta P \left[\hat{\mathcal{R}}_j \Psi - \mathbf{T}_j^{(1)} \right] \right\} \right] , \quad (27)$$

where D_t and D_r are the orientationally averaged *translational* diffusion coefficient and the *rotational* diffusion coefficient of a single, non-interacting rod, respectively, with $\hat{\mathbf{I}}$ the identity tensor, and Ψ is the total energy due to rod-rod interactions. The force and torque due to the action of the external electric field on single rods are denoted as $\mathbf{F}_j^{(1)}$ and $\mathbf{T}_j^{(1)}$, respectively. The forces and torques due to rod-rod interactions are incorporated through the total potential energy Ψ. Note that the orientational dependence of the single-particle translational diffusion coefficient is described by the tensor $\hat{\mathbf{I}} + \hat{\mathbf{u}}_j \hat{\mathbf{u}}_j$, which assumes long and thin rods. Furthermore, ∇_j is the gradient operator with respect to $\mathbf{r}_j$ and,

$$\hat{\mathcal{R}}_j \, (\cdots) \; = \; \hat{\mathbf{u}}_j \times \nabla_{\hat{\mathbf{u}}_j} \, (\cdots) \; ,$$

is the "rotation operator", with $\nabla_{\hat{\mathbf{u}}_j}$ the gradient operator with respect to the Cartesian coordinates of $\hat{\mathbf{u}}_j$.

The one-particle pdf $P(\hat{\mathbf{u}}, t)$ for the orientation $\hat{\mathbf{u}}$ of a rod can be found from the N-particle pdf by integration with respect to all position coordinates and orientations, except for $\hat{\mathbf{u}}_1 \equiv \hat{\mathbf{u}}$,

$$P(\hat{\mathbf{u}}, t) \; = \; \int d\mathbf{r}_1 \int d\mathbf{r}_2 \cdots \int d\mathbf{r}_N \times \oint d\hat{\mathbf{u}}_2 \cdots \oint d\hat{\mathbf{u}}_N \; P(\mathbf{r}_1, \mathbf{r}_2, \cdots, \mathbf{r}_N, \hat{\mathbf{u}}, \hat{\mathbf{u}}_2, \cdots, \hat{\mathbf{u}}_N, t) \, .$$

Assuming a pair-wise additive potential,

$$\Psi \; = \; \sum_{i>j} V(\mathbf{r}_i - \mathbf{r}_j, \hat{\mathbf{u}}_i, \hat{\mathbf{u}}_j, t) \; ,$$

where V is the pair-interaction potential, integration of the Smoluchowski equation (27) gives,

$$\frac{\partial}{\partial t} P(\hat{\mathbf{u}}, t) \; = \; D_r \hat{\mathcal{R}} \cdot \left\{ \hat{\mathcal{R}} P(\hat{\mathbf{u}}, t) - \beta \, P(\hat{\mathbf{u}}, t) \left[\mathbf{T}^{eff}(\hat{\mathbf{u}}, t) + \mathbf{T}^{(1)}(\hat{\mathbf{u}}, t) \right] \right\} \; , \quad (28)$$

with $\hat{\mathcal{R}}$ the rotational operator with respect to $\hat{\mathbf{u}}$, and where the *effective torque* is equal to,

$$\mathbf{T}^{eff}(\mathbf{r}, \hat{\mathbf{u}}) \; = \; - \int d\mathbf{r}' \oint d\hat{\mathbf{u}}' \, \rho(\mathbf{r}', \hat{\mathbf{u}}', t) \times g(\mathbf{r}, \mathbf{r}', \hat{\mathbf{u}}, \hat{\mathbf{u}}') \hat{\mathcal{R}} V(\mathbf{r} - \mathbf{r}', \hat{\mathbf{u}}, \hat{\mathbf{u}}') \, . \quad (29)$$

Here, the pair-correlation function g is defined as,

$$P(\mathbf{r}, \mathbf{r}', \hat{\mathbf{u}}, \hat{\mathbf{u}}, t) \; = \; P(\mathbf{r}, \hat{\mathbf{u}}, t) \, P(\mathbf{r}', \hat{\mathbf{u}}', t) \, g(\mathbf{r}, \mathbf{r}', \hat{\mathbf{u}}, \hat{\mathbf{u}}', t) \; ,$$

with $P(\mathbf{r}, \mathbf{r}', \hat{\mathbf{u}}, \hat{\mathbf{u}}', t)$ the two-particle pdf for the coordinates $\{\mathbf{r}, \hat{\mathbf{u}}\}$ and $\{\mathbf{r}', \hat{\mathbf{u}}'\}$ of two rods (for mathematical details of the derivation of eq.(28), see Ref.[71]). The effective torque on a rod with its center at $\mathbf{r}$ and with orientation $\hat{\mathbf{u}}$ is the torque exerted by a second rod, averaged over it's position $\mathbf{r}'$ and orientation $\hat{\mathbf{u}}'$.

Onsager showed that the expression,

$$g(\mathbf{r}, \mathbf{r}', \hat{\mathbf{u}}, \hat{\mathbf{u}}') \; = \; \exp\left\{ -\beta \, V(\mathbf{r} - \mathbf{r}', \hat{\mathbf{u}}, \hat{\mathbf{u}}') \right\} \; , \quad (30)$$

which is generally valid for very dilute colloidal systems, is also asymptotically exact for *concentrated* systems of very long and thin, hard rods in equilibrium, to within the nematic phase, provided that the degree of alignment is not very high [72, 73] (see also the appendix in Ref.[71]). Onsager's arguments for the validity of eq.(30) also holds for repulsive charged rods, as long as the Debye length is very small as compared to the rod length (but not necessarily small compared to the core diameter). Using eq.(30) as an approximation for the present analysis assumes, (i) that attractive electrostatic interactions resulting from polarization charges are weaker than the repulsive interactions of non-polarized rods, and (ii) that non-equilibrium contributions are small. Assumption (ii) relies on the fact that during a cycle of the external field, the relative positions and orientations of the rods are essential unchanged. For sufficiently high frequencies, the time dependent interaction potential can be averaged over a cycle of the external field, as already discussed before. The time-averaged interaction potential can then be treated as an equilibrium potential, for which Onsager's result in eq.(30) applies. The evaluation of non-equilibrium contributions to the approximation (30) is a formidable task by itself, and is beyond the scope of the present analysis.

Substitution of the approximation (30) into eq.(29) leads to,

$$\mathbf{T}^{eff}(\hat{\mathbf{u}}, t) \; = \; -\hat{\mathcal{R}} \, V^{eff}(\hat{\mathbf{u}}, t) \; , \quad (31)$$

where *the effective potential* V^{eff} is equal to (with $\mathbf{R} = \mathbf{r}' - \mathbf{r}$),

$$\beta \, V^{eff}(\hat{\mathbf{u}}, t) \; = \; - \int d\mathbf{R} \oint d\hat{\mathbf{u}}' \, P(\mathbf{R}, \hat{\mathbf{u}}', t) \, \exp\left\{ -\beta \, V(\mathbf{R}, \hat{\mathbf{u}}, \hat{\mathbf{u}}') \right\} \; . \quad (32)$$

The interaction potential is equal to,

$$\begin{aligned} & V(\mathbf{R}, \hat{\mathbf{u}}, \hat{\mathbf{u}}') \\ & \quad = \infty \qquad\qquad\qquad\qquad , \text{ for core overlap} \, , \\ & \quad = \bar{V}_{EE}(\mathbf{R}, \hat{\mathbf{u}}, \hat{\mathbf{u}}') + V_{\bar{Q}\bar{Q}}(\mathbf{R}, \hat{\mathbf{u}}, \hat{\mathbf{u}}') \; , \text{ no core overlap} \, , \end{aligned}$$

where "core overlap" refers to the overlap of the hard cores of two rods, and $\bar{V}_{EE}$ is the cycle-averaged electrostatic potential (26) that results from polarization charge interactions, and $V_{\bar{Q}\bar{Q}}$ is the potential (24) due to unpolarized charge interactions. Since,

$$\int d\mathbf{R} \oint d\hat{\mathbf{u}}' \, P(\mathbf{R}, \hat{\mathbf{u}}') \; = \; 1 \; ,$$

while the effective torque is a derivative of the effective potential, eq.(32) for the potential can be rewritten as,

$$V^{eff}(\hat{\mathbf{u}},t) \;=\; V_{hc}^{eff}(\hat{\mathbf{u}},t) + V_{Q}^{eff}(\hat{\mathbf{u}},t)\;, \tag{33}$$

where,

$$\beta\, V_{hc}^{eff}(\hat{\mathbf{u}},t) \;=\; \oint d\hat{\mathbf{u}}\,' \int_{V_c(\hat{\mathbf{u}},\hat{\mathbf{u}}\,')} d\mathbf{R}\; P(\mathbf{R},\hat{\mathbf{u}}\,',t) \tag{34}$$

is the contribution due to hard-core interactions, while,

$$\beta\, V_{Q}^{eff}(\hat{\mathbf{u}},t) \;=\; \oint d\hat{\mathbf{u}}\,' \int_{\bar{V}_c(\hat{\mathbf{u}},\hat{\mathbf{u}}\,')} d\mathbf{R}\; P(\hat{\mathbf{u}}\,',t) \tag{35}$$
$$\times\left[1-\exp\left\{-\beta\left[\bar{V}_{EE}(\mathbf{R},\hat{\mathbf{u}}\,,\hat{\mathbf{u}}\,')+V_{\bar{Q}\bar{Q}}(\mathbf{R},\hat{\mathbf{u}}\,,\hat{\mathbf{u}}\,')\right]\right\}\right],$$

is the effective potential arising from charge interactions. Here, $V_c(\hat{\mathbf{u}},\hat{\mathbf{u}}')$ is the volume in $\mathbf{R}$-space where the cores of two rods with orientations $\hat{\mathbf{u}}$ and $\hat{\mathbf{u}}'$ overlap, and $\bar{V}_c(\hat{\mathbf{u}},\hat{\mathbf{u}}')$ where there is no overlap. Note that the effective potentials are time dependent as a result of melting of nematic order, and does not refer to the frequency with which the external field oscillates. As mentioned before, the frequency of the external field is sufficiently high that rods do not change their configuration during a cycle of the external field, so that instantaneous interaction potentials can be time-averaged over a cycle-time.

B. Evaluation of the potentials V_{hc}^{eff} and V_{Q}^{eff}

In the derivation of equations of motion for the order-parameter density from the Smoluchowski equation, further approximations have to be made. Upon evaluation of the integrals in eqs.(34,35) for the effective potentials, the combinations $|\,\hat{\mathbf{u}}\times\hat{\mathbf{u}}\,'\,|$ and $|\,\hat{\mathbf{u}}\times\hat{\mathbf{u}}\,'\,|\;\ln|\,\hat{\mathbf{u}}\times\hat{\mathbf{u}}\,'\,|$ are encountered (see appendices A and B for mathematical details). These functions are expanded with respect to the orientational order parameter, with the neglect of terms of fourth-order. Such an expansion allows for the evaluation of the effective potentials in terms of the orientational order parameter tensor $\mathbf{S}$ (the brackets denote ensemble averaging),

$$\mathbf{S} \;=<\hat{\mathbf{u}}\,\hat{\mathbf{u}}>=\;\oint d\hat{\mathbf{u}}\;\hat{\mathbf{u}}\,\hat{\mathbf{u}}\,P(\hat{\mathbf{u}},t)\;, \tag{36}$$

which is the central quantity of interest. An equation of motion for this tensor is derived in the next subsection from the Smoluchowski equation, after the present evaluation of the effective potentials. The largest eigenvalue λ of $\mathbf{S}$ measures the degree of orientational order. The Ginzburg-Landau type of expansion gives rise to the well-know Maier-Saupe approximation for the effective hard-core interaction potential [71], and reproduces the lower- and upper-spinodal concentrations as obtained by Onsager for hard-core rods [72, 73]. The mathematical details for the explicit evaluation of the effective hard-core potential in terms of the orientational order parameter are given in appendix A, and for the charge interactions in appendix B.

Applying the above mentioned Ginzburg-Landau expansion with respect to the orientational order parameter to eq.(34) for the hard-core potential leads to the Maier-Saupe potential (see appendix A),

$$\beta\, V_{hc}^{eff}(\hat{\mathbf{u}},t) \;=\; \frac{21\,\pi}{32}\,dL^2\,\bar{\rho} - \frac{15\pi}{32}\,dL^2\,\bar{\rho}\,\hat{\mathbf{u}}\,\hat{\mathbf{u}}:\mathbf{S}(t)\,. \tag{37}$$

The next higher order contribution is of fourth order in the orientational order parameter λ. As before, d is the diameter and L the length of the core of the rods, while $\bar{\rho}$ is the number density of rods.

The potential in eq.(35) due to charge interactions consists of three contributions (see appendix B),

$$V_{Q}^{eff} \;=\; \Delta V_{Q,hc}^{eff} + V_{twist}^{eff} + V_{pol}^{eff}\;.$$

The physical interpretation and the mathematical form of these potentials are as follows:

(i) The term $\Delta V_{Q,hc}^{eff}$ is a contribution that is of the form of an effective hard-core potential, as in eq.(37). This contribution, added to the "bare" effective hard-core potential (37) gives rise to an effective diameter of the rods due to charge interactions, in the same spirit of Onsager [72, 73] and Refs.[74, 75] for *thin* double layers. Within the approximations discussed in appendix B, the effective diameter for *thick* double layers ($\kappa\, d \lesssim 1$) is given by,

$$\frac{d_{eff}}{d} \;=\; \frac{1}{\kappa\, d}\;\left[\,\ln\{K_Q\}+C\,\right]\;, \tag{38}$$

where $C \approx -3/4$. This contribution can thus be accounted for by replacing d by d_{eff} in eq.(37). Scaling of the effective diameter with the Debye length has also been found for line charges in Ref.[76], with a very similar prefactor that also depends logarithmically on the charge of the rod.

(ii) There is a "twisting potential" V_{twist}^{eff} that is due to interactions between the unpolarized charge density. This term accounts for the increase in energy when rods are aligned, due to an increased overlap of the electrical double layers, and is given by,

$$\beta\, V_{twist}^{eff}(\hat{\mathbf{u}},t) \;=\; -\frac{21\,\pi}{32}\,\left[\frac{57}{84}-\ln 2\right]\,\frac{L^2}{\kappa}\,\bar{\rho} \tag{39}$$
$$+\frac{15\pi}{32}\,\left[\frac{5}{4}-\ln 2\right]\,\frac{L^2}{\kappa}\,\bar{\rho}\,\hat{\mathbf{u}}\hat{\mathbf{u}}:\mathbf{S}\;.$$

Note that this is of the same form as the hard-core contribution in eq.(37), within the approximations discussed in appendix B. As will turn out in section VII, the twist effect never destabilizes the nematic state. It merely leads to a torque that will decrease nematic order. The "twisting effect" has been discussed for thin double layers in detail in Refs.[74, 75].

(iii) The third contribution is related to interactions between the polarization charges. This contribution V_{pol}^{eff} varies like $\sim E_0^4$, and is equal to,

$$\beta\, V_{pol}^{eff}(\mathbf{r},\hat{\mathbf{u}}) \;=\; -\,\frac{7\pi}{192}\,\bar{\rho}\,\frac{L^2}{\kappa}\,\left[\frac{K_E}{K_{\bar{Q}}}\right]^2 h(\Omega)\,\mathcal{E}_0^4 \times\Big(\hat{\mathbf{E}}_0\,\hat{\mathbf{E}}_0:\hat{\mathbf{u}}\,\hat{\mathbf{u}}\Big)\,\Big(\hat{\mathbf{E}}_0\,\hat{\mathbf{E}}_0:\mathbf{S}(\mathbf{r},t)\Big)\;,$$

with,

$$h(\Omega)=\left[\frac{1}{\Omega}\,\frac{\sin\{\Omega\}+\sinh\{\Omega\}}{[\cos\{2\,\Omega\}+\cosh\{2\,\Omega\}]^2}\right]^2\left[1+\tfrac{4}{3}\Omega^4+\tfrac{2}{5}\Omega^8\right]. \quad (40)$$

The frequency dependent function h is plotted in Fig.3c. This function vanishes at high frequencies as ions can not follow the electric field anymore.

C. The equation of motion for the order parameter tensor S

The equation of motion for the orientational order parameter tensor $\mathbf{S}$ is obtained by substitution of the potentials discussed in the previous subsection into the Smoluchowksi equation (28), in combination with eqs.(31,33) and the expression (7) for the single-particle torque. Multiplying both sides of the resulting equation of motion with $\hat{\mathbf{u}}\hat{\mathbf{u}}$ and subsequent integration with respect to $\hat{\mathbf{u}}$ leads to an equation of motion for $\mathbf{S}$, which however, also contains the fourth order average $\mathbf{S}^{(4)} =< \hat{\mathbf{u}}\hat{\mathbf{u}}\hat{\mathbf{u}}\hat{\mathbf{u}} >$. To obtain a closed equation of motion for $\mathbf{S}$, we used the following the closure relation,

$$\mathbf{S}^{(4)}:\mathbf{M} \;=\; \tfrac{1}{5}\,[\,\mathbf{S}\cdot\mathbf{M}+\mathbf{M}\cdot\mathbf{S} -\mathbf{S}\cdot\mathbf{S}\cdot\mathbf{M}-\mathbf{M}\cdot\mathbf{S}\cdot\mathbf{S}+2\,\mathbf{S}\cdot\mathbf{M}\cdot\mathbf{S}+3\,\mathbf{S}\,\mathbf{S}:\mathbf{M}\,]\;, \quad (41)$$

with $\mathbf{M}$ an arbitrary matrix. This closure relation is derived and discussed in Ref.[77]. The mathematical details for the derivation of the explicit equation of motion for $\mathbf{S}$ are discussed in appendix C. The equation of motion for $\mathbf{S}$ can be written in the form,

$$\frac{\partial\,\mathbf{S}}{\partial\,\tau} \;=\; \mathbf{\Delta}_{id}+\mathbf{\Delta}_{Q,hc}+\mathbf{\Delta}_{twist}+\mathbf{\Delta}_{pol}+\mathbf{\Delta}_{torque}\;, \quad (42)$$

with,

$$\tau \;=\; D_r\,t\;,$$

where $\mathbf{\Delta}_{id}$ is the contribution from free diffusion, $\mathbf{\Delta}_{Q,hc}$ stems from hard-core interactions (with an effective hard-core diameter that accounts for unpolarized charge interactions), $\mathbf{\Delta}_{twist}$ is the twist contribution, $\mathbf{\Delta}_{pol}$ is the contribution due to interactions from polarization charges, and $\mathbf{\Delta}_{torque}$ is the contribution of single-particle torques.

The contributions are given by (see appendix C for mathematical details),

$$\begin{aligned}
\mathbf{\Delta}_{id} &= 6\,\left[\,\tfrac{1}{3}\,\hat{\mathbf{I}}-\mathbf{S}\,\right]\;,\\
\mathbf{\Delta}_{Q,hc} &= \frac{9}{2}\,\frac{L}{d_{eff}}\,\varphi_{eff}\,\{\,\mathbf{S}\cdot\mathbf{S}-\mathbf{S}\,\mathbf{S}:\mathbf{S}\,\}\;,\\
\mathbf{\Delta}_{twist} &= -\,\frac{9}{2}\,\left[\frac{5}{4}-\ln 2\right]\,\frac{1}{\kappa\,d_{eff}} \times\frac{L}{d_{eff}}\,\varphi_{eff}\,\{\,\mathbf{S}\cdot\mathbf{S}-\mathbf{S}\,\mathbf{S}:\mathbf{S}\,\}\;,\\
\mathbf{\Delta}_{pol} &= \frac{7}{60}\,\left[\frac{K_E}{K_Q}\right]^2\,\frac{1}{\kappa\,d_{eff}} \times\frac{L}{d_{eff}}\,\varphi_{eff}\,h(\Omega)\,\mathcal{E}_0^4\,\Big(\mathbf{S}:\hat{\mathbf{E}}_0\hat{\mathbf{E}}_0\Big)\,\mathbf{F}(\mathbf{S},\hat{\mathbf{E}}_0)\;,\\
\mathbf{\Delta}_{torque} &= \frac{1}{80\,z^2}\,\frac{L}{l_B}\,\tilde{F}\,I(\Omega)\,\mathcal{E}_0^2\,\mathbf{F}(\mathbf{S},\hat{\mathbf{E}}_0)\;, \qquad (43)
\end{aligned}$$

where $\hat{\mathbf{E}}_0$ is the unit vector along the direction of the external field, where the effective diameter is given in eq.(38), and where the corresponding effective volume fraction is defined as,

$$\varphi_{eff} \;=\; \frac{\pi}{4}\,d_{eff}^2\,L\,\bar{\rho}\;,$$

where, as before, $\bar{\rho}$ is the number density of rods. The effective diameter and volume fraction are larger than their corresponding bare values for the hard-core diameter and hard-core volume fraction, respectively, due to charge-charge interactions (in the absence of the external field). These effective parameters depend crucially on the ionic strength through their dependence on the Debye length, which will turn out to be essential for the existence of the dynamical state. Furthermore, the frequency-independent quantity $\tilde{F}$ is defined as (with $F_1(\Omega)$, F_3, and $I(\Omega)$ given in eq.(9)),

$$\tilde{F} \;=\; F_1(\Omega)\,F_3/I(\Omega)\;,$$

while,

$$\mathbf{F}(\mathbf{S},\hat{\mathbf{E}}_0) \;\equiv\; \tfrac{3}{2}\,\mathbf{S}\cdot\hat{\mathbf{E}}_0\hat{\mathbf{E}}_0+\tfrac{3}{2}\,\hat{\mathbf{E}}_0\hat{\mathbf{E}}_0\cdot\mathbf{S}+\mathbf{S}\cdot\mathbf{S}\cdot\hat{\mathbf{E}}_0\hat{\mathbf{E}}_0 +\hat{\mathbf{E}}_0\hat{\mathbf{E}}_0\cdot\mathbf{S}\cdot\mathbf{S}-2\,\mathbf{S}\cdot\hat{\mathbf{E}}_0\hat{\mathbf{E}}_0\cdot\mathbf{S}-3\,\mathbf{S}\,\mathbf{S}:\hat{\mathbf{E}}_0\hat{\mathbf{E}}_0\;, \quad (44)$$

is introduced for brevity.

The above equations of motion can be used to calculate the location of binodals and spinodals (see section VI), and describe the melting dynamics of the nematic below the lower-binodal concentration.

D. Domain growth within the meta-stable two-phase region

As the Debye increases due to re-condensation and the systems enters the two-phase region and becomes meta-stable. It would be an enormous task to set up a (semi-)quantitative theory for the growth kinetics of nematic

domains from the meta-stable region with a precision that is comparable to the melting kinetics as described in the previous subsections. Higher order terms in an expansion with respect to the orientational order parameter are required in a description of phase separation kinetics starting in the meta-stable region. Such an endeavor is beyond the scope of the present work. We will be satisfied with a simple semi-empirical approach. In Ref.[78] (see especially Fig.3 in this reference) it has been shown that the growth of the order parameter is in good approximation exponential in time, up to times where the order parameter is approaching its saturation value quite closely. During this time, the interface is quite diffuse, so that anchoring effects can be neglected. In fact, anchoring effects at domain walls can probably be neglected in the experiments on fd-virus suspensions at low ionic strength, also at the very late stages of growth, as the observed interface is quite diffuse [30, 31]. The exponential growth kinetics is captured by the simple kinetic equation,

$$\frac{\partial \mathbf{S}}{\partial \tau} \;=\; \frac{\bar{\mathbf{S}} - \mathbf{S}}{\mathcal{T}} + \mathbf{\Delta}_{pol} + \mathbf{\Delta}_{torque} \;, \qquad (45)$$

where $\bar{\mathbf{S}}$ is the order parameter tensor of the nematic phase in equilibrium, without the electric field, and where $\mathcal{T}$ is the time scale on which domains increase their internal nematic order. The time scale $\mathcal{T}$ serves, within the present approach, as a free parameter that should attain values that are in agreement with growth rates observed experimentally. The first term in eq.(45) describes the growth kinetics in the absence of the field (similar to the first three terms in eq.(42) for the melting kinetics), while the last two terms incorporate the effect of field-induced torques and interactions.

V. A MODEL FOR DISSOCIATION/ASSOCIATION OF CONDENSED IONS AND IT'S EFFECT ON IONIC STRENGTH

As already indicated in section II, the above equations of motion do not exhibit oscillatory behaviour (also when reasonable approximations for the hydrodynamic torque due to bending [22] are added), and always give rise to a time-independent, stationary solution for $\mathbf{S}$. What is neglected so far is the possibility that condensed ions can dissociate from, and associate to, the surfaces of rods. As argued in section II, release and re-condensation of ions is essential for the observed melting and forming of nematic domains in the D-state.

Due to the field-induced polarization of the layer of condensed ions, there is an excess of condensed ions as compared to the unpolarized state on one half of the rod, while at the same instant there is a reduction on the other half of the core of the rod. Condensed ions tend to dissociate into the solvent when there is an excess concentration of condensed ions, while condensation will occur when there is a reduction as compared to the surface concentration in the absence of the external field. When the concentration of condensed ions differs from the equilibrium concentration, the resulting polarization induced electric field perpendicular to the rod either pushes condensed ions into the solvent, or attracts ions from the solvent towards the condensed layer (see the sketch in Fig.5a). The same mechanism of association/dissociation of condensed ions has been proposed in Refs.[79], on the basis of which the saturation of the induced dipole moment in a DC electric field of DNA strands with different lengths can be understood.

The amount of ions that is released per unit time is proportional to the local excess concentration of condensed ions and the local electric field strength perpendicular to the cylindrical axis (except for a small contribution at the tip of the rod). The latter field strength is proportional to the excess charge density. The flux of condensed ions towards the solvent at positions where there is an excess of condensed ions, averaged over a cycle of the external field, is therefore proportional to the total squared excess charge density $\left(R^{'}_{c,\,\|}\right)^2 + \left(R^{''}_{c,\,\|}\right)^2$. The same holds for the association of condensed ions on that part of the core where there is a shortage of condensed ions. The field strength that pulls ions to the rod surface as well as the concentration near the outer part of the condensed layer are proportional to the excess charge density. The proportionality constants for dissociation and association are different, also because the concentration in the inner part and the outer part of the condensed layer are not the same. The rate-of-change of the number of condensed ions, averaged over a cycle of the external field, is thus found from integration of the expressions (5) for the induced charges densities to be equal to (using eq.(3) for κ_c) (as before, $\tau = D_r\, t$),

$$\frac{d\,N_c}{d\tau} \;=\; -\,\mathcal{C}_d\,N_c^2\,\left(\frac{z^2\,l_B}{L\,[\,1+2\,\kappa_c\,a\,\mathcal{K}(\kappa\,a)\,]}\right)^2\,\mathcal{E}_0^2 \times\,\left(\hat{\mathbf{E}}_0\hat{\mathbf{E}}_0 : \mathbf{S}(t)\right)\,I(\Omega)\;, \qquad (46)$$

where the function $I(\Omega)$ (that also describes the frequency dependence of single-particle torques) is given in eq.(9). This function is plotted in Fig.3c. The constant C_d will be referred to as the (effective) *dissociation constant*. As there is no microscopic theory available that allows for the calculation of C_d, this constant will be used as an adjustable parameter when a comparison to experiments is made.

When a rod is to some extent oriented perpendicular to the external field, the layer of condensed ions will also be polarized in the direction perpendicular to the long axis of the rod (see Fig.5b). This leads to an internal electric field that pulls the condensed ions that are in excess, back towards the surface of the rod (as indicated by the green arrows in Fig.5b). The release of condensed ions due to parallel polarization therefore diminishes as the perpendicular polarization increases. We

account for this by introducing a threshold for the orientational order along the field direction, below which no ion release occurs, but re-condensation takes place (a similar threshold field amplitude has been introduced in Ref.[79], although on the basis of different arguments related to thermal fluctuations of the number of condensed ions). Formally this is implemented by replacing $\mathbf{S}$ in eq.(46) by $\mathbf{S} - \alpha_{thr}\,\hat{\mathbf{E}}_0\hat{\mathbf{E}}_0$, where the numerical (positive) value of α_{thr} sets the threshold for dissociation. What is observed experimentally is that the dynamical state persists on increasing the electric field strength. Without the orientational threshold ($\alpha_{thr} = 0$), there will be certain field strength above which the system becomes isotropic, contrary to what is observed. The ionic strength then increased to an extent that the nematic remains unstable, and the isotropic state persists.

There is an un-physical feature of the equation of motion (46). Since the right hand-side is always negative, this equation implies that for a fixed orientation of a rod, all condensed ions will eventually dissociate. What has not been taken into account in the arguments leading to this result is that when sufficient ions are dissociated there will be a quasi-stationary state where the association of condensed ions on one half of the rod is as fast as the dissociation at the other half of the rod. The equation of motion (46) only describes the *initial stages* of ion release. The limiting number N_{lim} of condensed ions after a long time, keeping the orientation of the rods fixed, will decrease with the squared external field strength component along the rods long axis, since that field strength sets the potential perpendicular to the rods surfaces which drives the overall dissociation. On average, the quantity that sets the limiting number of condensed ions is therefore $\sim \mathcal{E}_0^2 \left(\hat{\mathbf{E}}_0\hat{\mathbf{E}}_0 : \mathbf{S}\right) I(\Omega)$, where, according to eq.(46), $I(\Omega)$ describes the effectiveness of the field due to the finite diffusivity of the ions. In addition, the number of condensed ions should be equal to $N_{c,\,0}$ (the number of ions without the field) for very low field amplitudes, while it should become formally equal to zero for large field strengths. The simplest form for the limiting number of condensed ions that complies with these requirements is,

$$N_{lim} \;=\; \frac{\alpha_{lim}\, N_{c,\,0}}{\alpha_{lim} + \mathcal{E}_0^2 \left(\hat{\mathbf{E}}_0\hat{\mathbf{E}}_0 : \mathbf{S}\right) I(\Omega)} \;,$$

where α_{lim} is an adjustable parameter. To ensure that, for a given orientation, the number of condensed ions indeed takes the value N_{lim} after long times, N_c^2 in eq.(46) is replaced by $N_c^2 - N_{lim}^2$. Note that this expression for the limiting number of condensed ions is only applicable for orientations towards the electric field for which the above described threshold for dissociation is reached. For orientations below the threshold we have,

$$N_{lim} \;=\; N_{c,0} \quad , \quad \text{when} \quad , \quad (\mathbf{S} : \hat{\mathbf{E}}_0\hat{\mathbf{E}}_0) < \alpha_{thr} \;,$$

since for such orientations no dissociation occurs, by definition.

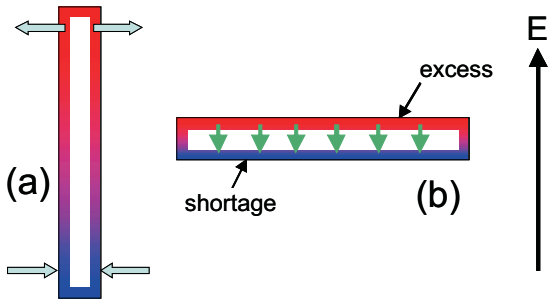

FIG. 5: (a) Polarization of the layer of condensed ions parallel to the rods long axis leads to an internal electric field that drives condensed ions into the solvent when there is an excess of ions (indicated in red). In case of a shortage of condensed ions (indicated in blue), ions from the solution tend to condense in order to restore equilibrium. (b) Perpendicular polarization creates an internal electric field that pulls the excess condensed ions back to the rods surface, as indicated by the green arrows.

We thus finally arrive at the following expression for the time-rate of change of the number of condensed ions,,

$$\frac{d\,N_c}{d\tau} \;=\; \pm\,\mathcal{C}_d\,\left\{\,N_c^2 - N_{lim}^2\,\right\}\left(\frac{z^2 l_B}{L\,[1+2\,\kappa_c\,a\,\mathcal{K}(\kappa\,a)]}\right)^2 \times \mathcal{E}_0^2\,\left(\hat{\mathbf{E}}_0\hat{\mathbf{E}}_0 :\, \left[\mathbf{S}(t) - \alpha_{thr}\,\hat{\mathbf{I}}\right]\right)\, I(\Omega)\;, \quad (47)$$

where the "+" applies when $(\mathbf{S} : \hat{\mathbf{E}}_0\hat{\mathbf{E}}_0) < \alpha_{thr}$, and the "−" applies otherwise.

It needs some time before the ion concentration within the bulk of the solvent is affected by the released condensed ions. Ions that dissociate from the condensed layer need to diffuse over typical distances of a few rod lengths in order to render a change in the homogeneous bulk concentration of ions. Similarly, it takes some time for ions to diffuse from the bulk towards the rods surface from the solvent bulk as ions associate to the condensed layer. The change of the bulk concentration of ions at time t is, in first approximation, therefore proportional to the number $\Delta N_c = N_{c,\,0} - N_c$ of released ions at time $t - \tau_{dif}$, where τ_{dif} is of the order of the time needed for ions to diffuse over distances equal to a few rod lengths. The time-dependent (inverse) Debye length at time t is therefore taken equal to (see eq.(1)),

$$\kappa(t) \;=\; \sqrt{\frac{2\,\beta\,e^2\,\left[\,c_0 + \bar{\rho}\,\Delta N_c(t - \tau_{dif})\,\right]}{\epsilon}}\;, \quad (48)$$

where $\bar{\rho}$ is the number density of rods. The effective diameter in eq.(38) is now also a time-dependent quantity equal to,

$$\frac{d_{eff}(t)}{d} \;=\; \frac{1}{\kappa(t)\,d}\,\left[\,\ln\{K_Q(\kappa \equiv \kappa(t))\} + C\,\right]\;, \quad (49)$$

where the interaction strength K_Q in eq.(25) is to be evaluated with an inverse Debye length equal to $\kappa(t)$.

The Debye length thus changes due to the release of condensed ions with a certain time lag, which affects the effective diameter with the same time lag. The change of the effective diameter changes the location of phase boundaries in a cyclic manner as release and recondensation occurs, which is at the origin of the dynamical state as explained on an intuitive level in section II.

VI. BINODAL AND SPINODAL CONCENTRATIONS

To solve the equations of motion, with the inclusion of of dissociation of condensed ions, it is necessary to know the location of the lower binodal concentration. Below the effective lower binodal concentration, melting occurs according to the equations of motion derived in section IV, while above the binodal, nematic order increases as discussed in subsection 45. The location of phase boundaries is therefore essential for the numerical solution of the equations of motion that we derived above.

For uncharged rods, the upper spinodal concentration can be found analytically from a stability analysis of the equation of motion (43), where only the terms $\mathbf{\Delta}_{id}$ $\mathbf{\Delta}_{Q,hc}$ contribute, and where $d_{eff} = d$ and $\varphi_{eff} = \varphi$. The upper spinodal concentration is found to be equal to $(L/d)\varphi = 4$, in accordance with Onsager's exact asymptotic result for long and thin hard rods [72, 73]. The lower spinodal concentration can be obtained numerically from the same equation of motion (43), and is found to be equal to $(L/d)\varphi = 3.556\cdots$.

For charged rods, a numerical solution of the equation of motion (43) for the order parameter reveals that the electric-field contributions $\mathbf{\Delta}_{pol}$ and $\mathbf{\Delta}_{torque}$ change spinodal concentrations less then 0.5 % for the maximum electric field strengths of $10\,V/mm$ that are applied in the experiments. This very small effect of the electric field on the location of phase-boundary concentrations can be neglected.

To obtain the lower and upper spinodal and binodal concentrations for charged rods, including the twist effect, we make use of the fact that the twist contribution and the effective hard-core contribution to the equation of motion (43) have the same dependence on the order parameter. This allows to calculate the binodal concentrations directly from the Onsager binodal concentrations ($(L/d)\varphi = 3.290$ and 4.191, respectively [75]), by the identification,

$$\left[\frac{L}{d}\,\varphi\right]_{Onsager} = \frac{L}{d_{eff}}\,\varphi_{eff}\left\{1-\left[\frac{5}{4}-\ln 2\right]\frac{1}{\kappa\, d_{eff}}\right\}. \quad (50)$$

The spinodal and binodal fd-virus concentrations in units of mg/ml can be obtained from a simple numerical evaluation of the right hand-side using eq.(38), together with the length $L = 880\,nm$ and thickness $d = 6.8\,nm$ of the fd-virus particles, as well as the connection $\varphi = 0.0011 \times [fd]$ between the hard-core volume fraction φ and the fd-concentration $[fd]$ in mg/ml. The spinodal concentrations can be obtained from the numerical solution of the equation of motion for $\mathbf{S}$, which gives the same result.

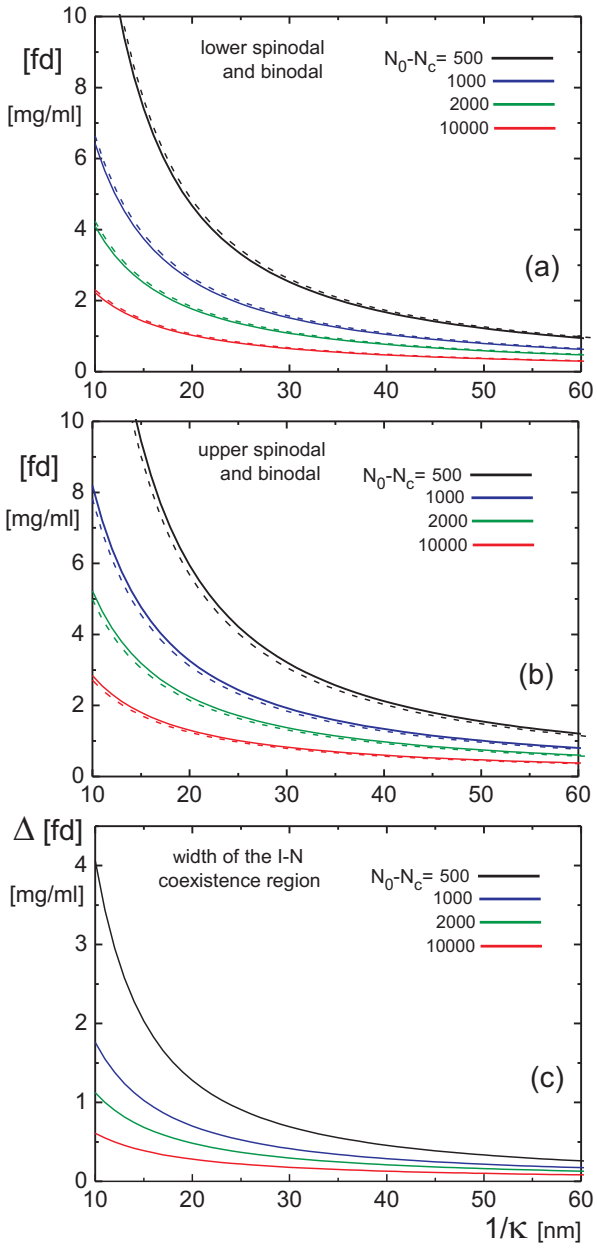

FIG. 6: (a) The location of the *lower* spinodal (dashed lines) and binodal (solid lines) concentrations as a function of the Debye length for various values of $N_0 - N_c$. (b) The same as in (a), but now for the *upper* spinodal and binodal concentrations. (c) The width of the I-N coexistence region. The parameters chosen here relate to fd-virus particles.

Since d_{eff} depends on the Debye length κ^{-1} and the difference $N_0 - N_c$ between the total number N_0 of immobile charges on the rod minus the number N_c of con-

densed ions, the location of spinodal and binodal concentrations depend on these two independent parameters. The location of the *upper* spinodal and binodal concentrations is given in Fig.6a (the dashed and solid lines, respectively), as a function of the Debye length for various values of $N_0 - N_c$. Similar plots for the *lower* spinodal and binodal concentrations are given in Fig.6b, while the width of the coexistence region is given in Fig.6c. As can be seen, the width of the coexistence region increases when the Debye length is decreased, in accordance with what is seen experimentally. The twist effect has a pronounced effect on the width of the coexistence region, as has been predicted before for thin double layers [74, 75].

Detailed experiments on the location of isotropic-nematic binodals for fd-viruses and their mutants, as a function of the persistence length and ionic strength (larger than $5\,mM$), can be found in Ref.[41]. Note that the present theory can not be applied at these relatively high ionic strengths, as our expressions for the effective diameter and the twist effect are only applicable for thick double layers.

VII. NUMERICAL RESULTS AND COMPARISON TO EXPERIMENTS

The length of the fd-core is $L = 880\ nm$, the bare core thickness is $d = 6.8\ nm$, and the number of negative bare charges is equal to 8800. The number of mono-valent positively charged condensed ions as obtained from Manning's condensation theory is equal to 7500 [80, 81]. This amount of condensed ions is in reasonable agreement with the experimentally determined location of the lower and upper binodal concentrations (1.5 ± 0.2 and $3.4 \pm 0.5\ mg/ml$, respectively [82]) and the calculated locations in Fig.6. The concentrations of fd-virus particles for the experiments in Refs.[30, 31] are 2.0 and $2.8\,mg/ml$, corresponding to bare values of $(L/d)\varphi = 0.28$ and 0.39, respectively (where φ is the bare volume fraction). The $TRIS/HCl$ buffer concentration is $0.16\,mM$, corresponding to a total ion concentration of $0.25\,mM$ (without the electric field), and a Debye length of $27\,nm$ (CO_2 that dissolves from the air has to be taken into account for these low buffer concentrations [83]). The value of the orientational order parameter (the largest eigenvalue of $\mathbf{S}$) at the binodal concentration is found in experiments to be equal to $\lambda = 0.93$, which value is used in eq.(45) for the domain-growth dynamics [41, 83]. Numerical results turn out to be quite insensitive to the threshold value α_{thr} in eq.(47) that sets the orientation of the rod along the field direction beyond which ion release occurs, which is chosen as $\alpha_{thr} = 1/2$. The time τ_{dif} between ion-release and the resulting increase of the bulk ionic strength is taken equal to the time needed for ions in solution to diffuse over ten rod lengths. The parameters that critically determine the location of the $N^\star$-to-D transition lines in the field-amplitude versus frequency plane, as well as the time scale on which melting and domain growth occurs as a function of the distance from the transition lines, are the time scale for domain growth $\mathcal{T}$ in eq.(45), the parameters α_{lim} and $\mathcal{C}_d$ in eq.(47) that set the dynamics of dissociation and association of condensed ions, and the bare diffusion coefficient D in eq.(2) for diffusion of condensed ions that includes friction with the core of the rod. A good comparison with experiments [30–32] is found when these values are chosen as $\mathcal{T} = 100$, $\alpha_{lim} = 1.2 \times 10^{-4}$, $\mathcal{C}_d = 2.0 \times 10^5$, and $D = D_0/290$ (where $D_0 = 2.0 \times 10^{-9}\,m^2/s$ is the diffusion coefficient of ions in solution). Note that the value for $\mathcal{T} = 100$ corresponds to a domain growth time of $100/D_r = 5\,s$, which is within the range of experimentally observed growth rates. The value of $D = D_0/290$ is not the same, but of similar order, as determined in Ref.[49] from a fit to birefringence experiments on fd-virus suspensions at very low fd-concentration and very low ionic strength, corresponding to a reported Debye length of $300\,nm$ [18].

The appropriate measure for the binodal and spinodal concentrations is the quantity on the right hand-side in eq.(50), to which we shall refer to as C^{eff}. When C^{eff} is smaller than the corresponding value of 3.290 for the lower binodal, the dynamics is gouverned by the equation of motion (42,43) that describes melting of nematic domains, while for larger values the dynamics is described by the domain-growth equation (45). Note that the isotropic state is meta-stable up to $C^{eff} = 4$, which corresponds to an effective concentration that is never reached during a cycle of melting and forming of nematic domains in the dynamical D-state. Hence, C_{eff} is calculated from the instantaneous ionic strength, on the basis of which either eq.(42,43) or (45) is used in a time step. For a given Debye length, the value of C^{eff} corresponds to an effective rod-concentration, which, for the fd-virus particles, we shall refer to as the *critical fd-concentration* $[fd]_{crit}$. This is the fd-concentration below which nematic domains melt, and above which nematic domains are formed. Since the Debye length is time dependent through the dissociation/association of condensed ions, this critical fd-concentration is also time dependent. In the dynamical state, the critical fd-concentration oscillates around the bulk fd-concentration of the dispersion.

With the above introduced values of the various parameters we find oscillations of the orientational order parameter λ (the largest eigenvalue of $\mathbf{S}$), as can be seen in Fig.7. The field amplitudes indicated in the figure are corrected for the dielectric polarization of the ITO-water interface, which renders the actual field amplitudes a factor 0.096 smaller than the applied field amplitudes. There is a growth of orientational order when the fd-concentration is larger than $[fd]_{crit}$, and a relatively fast decay towards the isotropic state (where $\lambda = 1/3$) otherwise. In addition, the period of oscillation is strongly depending on the distance from the $N^\star$-to-D transition line, which is located at $0.30\,V/mm$, and saturates to about $2\,s$ for high field amplitudes (this will be discussed in more detail below).

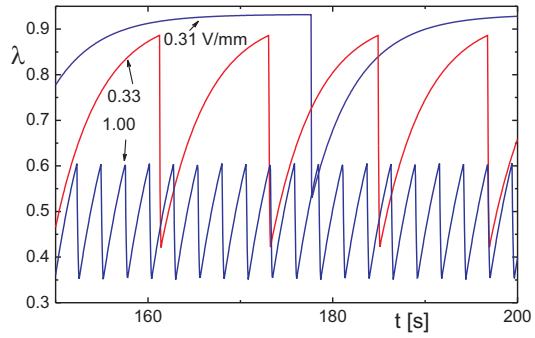

FIG. 7: Oscillations of the orientational order parameter λ for various field amplitudes at a fixed frequency of 200 Hz and a fd-concentration of 2.0 mg/ml (see the movies Movie-Ds for the slow dynamics and Movie-Df for the fast dynamics in the supplementary material).

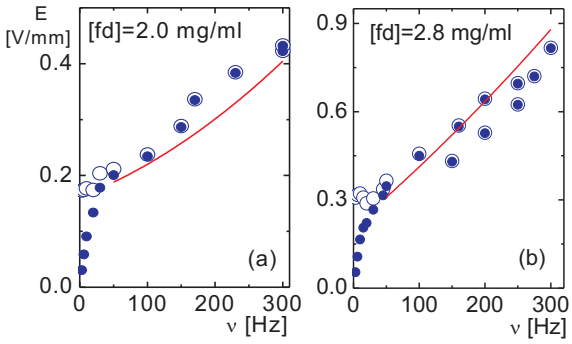

FIG. 8: The experimental and theoretical transition lines in the field-amplitude versus frequency plane, for fd-concentrations of (a) 2.0 and (b) 2.8 mg/ml. The open circles are experimental data only corrected for the ITO-water interface polarization, while the solid data are also corrected for electrode polarization. The red lines are the theoretical transition lines.

The location of the $N^\star$-to-D transition line are the points in the field amplitude versus frequency plane where the period of oscillation diverges, and no oscillations occur upon lowering the field amplitude. That the location $N^\star$-to-D transition line for the two fd-concentrations of 2.0 and 2.8 mg/ml is correctly reproduced by theory is show in Fig.8 (the solid red lines). Due to the assumption that the configuration of rods is essentially unaltered during a cycle of the external field, the theory is only valid for frequencies larger than a few tens of Hz. The transition lines are therefore calculated only for frequencies larger than 50 Hz. The open data points are corrected for ITO-solvent polarization only, while the filled data points are also corrected for electrode polarization.

In view of the frequency dependence of the polarization response functions an estimate can be made of the

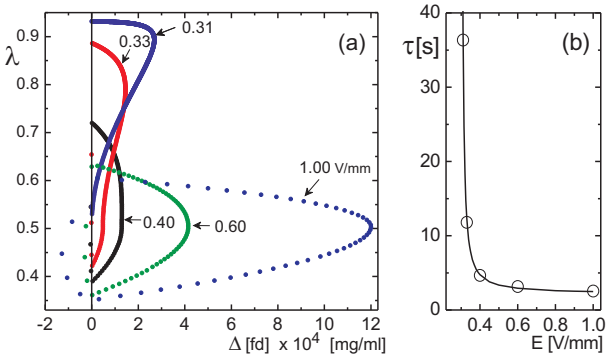

FIG. 9: (a) Limit cycles in the eigenvalue λ versus $\Delta[fd] = [fd] - [fd]_{crit}$ plane, with $[fd] = 2.0\,mg/ml$ the analytical fd-concentration, and $[fd]_{crit}$ the time-dependent concentration where the lower binodal is located. Limit cycles are shown for a frequency of 200 Hz, for various field amplitudes (corrected for the ITO-solvent interface polarization). Points are at equal time intervals of 0.05 s, and the cycles are traversed anti-clockwise. (b) The time-constant τ of limit cycles as a function of the field amplitude. The points correspond to the limit cycles shown in (a), and the line corresponds to the power-law given in the main text.

frequency beyond which polarization essentially ceases to occur (a possibly over-simplified estimate has been discussed section II). From the frequency dependence of the polarization response functions in Fig.3c it is found that polarization ceases to occur when $\Omega = (\Lambda_\parallel/2)^{1/2} \gtrsim 2$, where $\Lambda_\parallel = \omega\, L^2/4D^{\rm eff}$, with the effective diffusion coefficient given in eq.(2), and with the bare diffusion coefficient of the condensed ions being equal to $D \approx D_0/290$ (with D_0 the diffusion coefficient of ions in solution, while the factor 290 has been established in section VII, being due to friction of condensed ions with the core of fd-virus). For typical parameters applying to fd-virus particles, with a Debye length of 27 nm, it follows that the critical frequency beyond which polarization ceases to occur is $\nu \approx 670\ Hz$. This is in agreement with the experimentally observed frequency of $\approx 400-700\,Hz$ where the state diagram changes its form (see Fig.1), and again suggests that the homeotropic H-phase is stabilized by hydrodynamic interactions through electro-osmotic flow.

Limit cycles in the orientational order parameter λ versus $\Delta[fd]$ plane are given in Fig.9a, where $\Delta[fd] = [fd] - [fd]_{crit}$, with $[fd] = 2.0\,mg/ml$. Limit cycles are shown for various values of the electric field amplitude, up to field amplitudes very close to the $N^\star$-to-D transition line. The time interval between the points shown is 0.05 s. When $\Delta[fd] < 0$ nematic domains melt, and the orientational order parameter drops relatively fast to a value close to the isotropic value $\lambda = 1/3$. Re-condensation occurs for these low degrees of orientational order so that $\Delta[fd]$ becomes positive and nematic order increases. Above the threshold value for the order

parameter, dissociation of condensed ions takes places. The accompanied decrease of the Debye length leads to an increase of $[fd]_{crit}$ and hence to a decrease of $\Delta[fd]$. When $\Delta[fd]$ becomes negative the cycle repeats itself. This is the cycle that has been discussed on an intuitive level in section II. For field amplitudes close to the transition line the cycling times become large. From the form of the limit cycle in Fig.9a and the oscillatory behaviour shown in Fig.7 for the smallest field amplitude it can be concluded that the rate-limiting step is the release of condensed ions just before the domain becomes unstable. When the number of dissociated ions does not suffice to render the nematic unstable, the oscillations cease to occur, and the stable state is the $N^\star$-phase. The divergence of the cycling time on approach of the $N^\star$-to-D transition line that is observed experimentally is also seen in the theory, as shown in Fig.9b. The data points correspond to the limit cycles shown in Fig.9a, while the solid line is the power law dependance $\tau = 2.20 + 0.18 \times (\, E - 0.300\,)^{-1.15}$ for the cycling time τ. The exponent 1.15 and the saturation cycling time at high field strengths of $2.2\,s$ are in accordance with values found in experiments.

VIII. SUMMARY AND CONCLUSIONS

In a recent experiment where an oscillating external electric field is applied to a dispersion of rod-like colloids (fd-viruses) in the isotropic-nematic biphasic region, a dynamical state is observed [30, 31]. In this dynamical state, nematic domains melt and form on a seconds time scale. The origin of the dynamical state is attributed to the cyclic dissociation and association of condensed ions. When a nematic domain is aligned along the electric-field direction, the layer of condensed ions of each rod-like colloid is polarized, leading to an electric field perpendicular to the long axes of the rods that drives the condensed ions into solution. This leads to an increase of the ionic strength that renders the nematic domain unstable as the Debye length, and thereby the effective concentration, is decreased. The nematic domain thus melts, so that the alignment along the electric field is lost, leading to association of condensed ions. The subsequent increase of the effective concentration renders the molten isotropic state meta-stable. A nematic domain is thus formed which aligns along the field direction, leading again to release of condensed ions. This cycle of increased and decreased ionic strength is at the origin of the dynamical state.

A quantitative theory is developed that describes the *melting* of the nematic state. This theory is based on the Smoluchowski equation, including the field-induced rod-rod interactions and torques. These torques and rod-rod interactions are obtained from a theory for the polarization of the layer condensed ions, where it is assumed that the ions are essentially constrained to move over the surface of the rod-like colloids. An empirical equation of motion is used that describes the *growth* of nematic domains, based on what is observed in simulations in the absence of an external field [78], and a simple model is proposed for the field-induced dissociation and association of condensed ions. A comparison is made with experiments for two fd-virus concentrations. The numerical solution of the coupled equations of motion reproduce the experimentally observed characteristics of the dynamical state, including the location of the transition line from the chiral-nematic state to the dynamical state in the field-amplitude versus frequency plane, and the power-law divergence of cycling-time for melting and forming of domains on approach of the transition line. In forthcoming work we plan to compare the present theory with experiments at different ionic strengths and fd-concentrations.

The release of condensed ions on increasing the field amplitude also explains the N-to-$N^\star$ transition, where the normal (non-chiral) nematic transforms to a chiral nematic. At low ionic strength, the helical nature of the core of the fd-virus particles is screened by the relatively long-ranged electrostatic interactions, leading to a non-chiral nematic state. As the field amplitude is increased, the accompanied release of condensed ions leads to a decrease of the Debye length, so that the core-core interactions become significant. The helical structure of the fd-cores now gives rise to a chiral nematic, which is the equilibrium nematic state at higher ionic strengths in the absence of an electric field. Within the $N^\star$ phase the ionic strength is not large enough to render the nematic unstable. This occurs once the dynamical state is entered.

There are three points where the present theory can be improved. First of all, the nematic-domain growth could be analyzed on the basis of the Smoluchowski equation as well. This requires the extension of the Smoluchowski approach to include higher-order contributions in orientational order, which is necessary to describe growth kinetics from the meta-stable state. Secondly, we used a simple model for the dissociation/association of condensed ions. There is so far no (Poisson-Boltzmann) theory that quantitatively describes the dissociation/association of condensed ions due to electric-field induced polarization. Thirdly, the present theory neglects spatial gradients in orientational order, and is therefore not capable of predicting the domain-size dependence on the field amplitude and frequency, which is found in Ref.[32] to diverge at the critical point CP in Fig.1. In principle such gradients contributions can be included in the Smoluchowski-equation approach. Possible alternatives to a Smoluchowski-equation and Poisson-Boltzmann approach to address these issues could be an analysis based on Ornstein-Zernike integral equations for nematics with an appropriate closure relation (see, for example Refs.[84, 85]), or a dynamical density-functional approach (see, for example, Refs.[86–88]).

Appendix A: Approximate evaluation of V_{hc}^{eff}

In order to evaluate the **R**-integral in eq.(34), the coordinates $\{\alpha, x, x'\}$ are introduced,

$$\mathbf{R}(\alpha, x, x') \;=\; \alpha\, d\, \frac{\hat{\mathbf{u}} \times \hat{\mathbf{u}}'}{|\,\hat{\mathbf{u}} \times \hat{\mathbf{u}}'\,|} + \tfrac{1}{2}\, L\, x\, \hat{\mathbf{u}} + \tfrac{1}{2}\, L\, x'\, \hat{\mathbf{u}}' \;.$$

The new integration variables α, x and x' vary within $(-1, 1)$. The Jacobian of the coordinate transformation is $d\,(L/2)^2\;|\,\hat{\mathbf{u}} \times \hat{\mathbf{u}}'\,|$, so that,

$$\beta\, V_{hc}^{eff}(\hat{\mathbf{u}}, t) \;=\; 2\, d\, L^2\, \bar{\rho} \oint d\hat{\mathbf{u}}'\;\; |\,\hat{\mathbf{u}} \times \hat{\mathbf{u}}'\,|\;\, P(\hat{\mathbf{u}}', t) \;. \quad (51)$$

The cross product is expanded in terms of Legendre polynomials $P_{2n}(x)$, with $x = \hat{\mathbf{u}} \cdot \hat{\mathbf{u}}'$,

$$\begin{aligned} |\,\hat{\mathbf{u}} \times \hat{\mathbf{u}}'\,| \;&=\; \sqrt{1 - x^2} \\ &=\; \frac{\pi}{4}\, P_0(x) - \frac{5\pi}{32}\, P_2(x) - \frac{9\pi}{256}\, P_4(x) + \cdots \;. \end{aligned} \quad (52)$$

Since P_2 is on average first order in the orientational order parameter for both $\hat{\mathbf{u}}$ and $\hat{\mathbf{u}}'$, it is in total of second order. Similarly, P_4 is of fourth order and is therefore neglected. Hence, using that $P_0(x) = 1$ and $P_2(x) = \frac{1}{2}\,\big(3\,x^2 - 1\big)$, it is found that with the neglect of fourth order contributions,

$$|\,\hat{\mathbf{u}} \times \hat{\mathbf{u}}'\,| = \; \frac{21\pi}{64} - \frac{15\pi}{64}\, \hat{\mathbf{u}}\hat{\mathbf{u}} : \hat{\mathbf{u}}'\hat{\mathbf{u}}' \;.$$

Substitution into eq.(51) leads to eq.(37).

Appendix B: Approximate evaluation of V_{Q}^{eff}

In order to evaluate the potential V_{Q}^{eff} in eq.(35), the **R**-integral is evaluated in terms of the coordinates $\{\alpha, x, x'\}$, defined as,

$$\mathbf{R}(\alpha, x, x') \;=\; \alpha\, \kappa^{-1}\, \frac{\hat{\mathbf{u}} \times \hat{\mathbf{u}}'}{|\,\hat{\mathbf{u}} \times \hat{\mathbf{u}}'\,|} + \tfrac{1}{2}\, L\, x\, \hat{\mathbf{u}} + \tfrac{1}{2}\, L\, x'\, \hat{\mathbf{u}}' \;.$$

The variable α ranges from $(-\infty, -\kappa\, d)$ and $(\kappa\, d, \infty)$ for non core-overlap, while $-1 < x,\, x' < 1$. The latter assures that α_0 and β_0 in eqs.(18,19) remain within the range $(-p/2, p/2)$. The Jacobian of the transformation to these new coordinates is equal to $\kappa^{-1}\,(L/2)^2\;|\,\hat{\mathbf{u}} \times \hat{\mathbf{u}}'\,|$. It is readily verified from eq.(23) that,

$$\begin{aligned} S_1 \;&=\; \;\; \Omega\, x \;, \\ S_2 \;&=\; -\,\Omega\, x' \;. \end{aligned}$$

Hence, from eq.(35),

$$\begin{aligned} \beta\, V_{Q}^{eff}(\hat{\mathbf{u}}, t) \;&=\; \frac{L^2}{2\,\kappa}\, \bar{\rho} \oint d\hat{\mathbf{u}}'\;\; |\,\hat{\mathbf{u}} \times \hat{\mathbf{u}}'\,|\;\, P(\hat{\mathbf{u}}', t) \\ &\times \int_{-1}^{1} dx \int_{-1}^{1} dx' \int_{\kappa\, d}^{\infty} d\alpha\;\, [\,1 - \exp\{-A\, \exp\{-\alpha\}/\alpha\}\,] \;, \end{aligned}$$

where,

$$\begin{aligned} A \;&=\; \frac{1}{|\,\hat{\mathbf{u}} \times \hat{\mathbf{u}}'\,|}\, \{\, K_Q \\ &-\tfrac{1}{2}\, K_E\, \mathcal{E}_0^2\, \hat{u}_z\, \hat{u}'_z\;\, [\, G(\Omega x)\, G(\Omega x') + H(\Omega x)\, H(\Omega x')\,]\} \;. \end{aligned} \quad (53)$$

We thus have to find an approximation for the integral,

$$\begin{aligned} I(A) \;&\equiv\; \int_{\kappa\, d}^{\infty} d\alpha\;\, [\,1 - \exp\{-A\, \exp\{-\alpha\}/\alpha\}] \\ &\approx\; -\,\kappa\, d + \int_{0}^{\infty} d\alpha\;\, [\,1 - \exp\{-A\, \exp\{-\alpha\}/\alpha\}] \;. \end{aligned} \quad (54)$$

For the case of thick double layers, typical values of A are large due to overlap of double layers of several beads. We thus have to find an approximation for this integral for large values of A. For thin double layers, where the interaction between the two sections of the cores of the two rods on closest approach can be approximated as two flat plates, the interaction potential "per bead-pair" is equal to $A \exp\{-\alpha\}$, where α is the distance between the two surfaces, instead of $A\, \exp\{-\alpha\}/\alpha$ for the thick double layers under consideration here. The corresponding integral for the effective potential in the Smoluchowski equation for thin double layers is,

$$\int_{0}^{\infty} d\alpha\;\, [\,1 - \exp\{-A\, \exp\{-\alpha\}\,\}\,] \;\approx\; \ln\{A\} + \gamma_E \;,$$

for thin double layers ,

where $\gamma_E = 0.5772\cdots$ is Euler's constant. The approximation on the right hand-side is an asymptotic expansion for large values of A, and is accurate to within 1 % for $A > 2$ [72–75]. The reason why the leading term for large values of A scales like $\ln\{A\}$ is that the combination $A \exp\{-\alpha\}$ in the exponent is order unity when $\alpha \lesssim \ln\{A\}$, and rapidly tends to zero for larger values of α. In a very crude approximation one could replace the integrand by a step function that is unity for $\alpha < \ln\{A\}$ and zero otherwise, which indeed leads to the leading order $\sim \ln\{A\}$ contribution. Similar to the case of a thin double layer, we can replace the integrand in eq.(54) by a step function which jumps from unity to zero for $A \exp\{-\alpha\}/\alpha = 1$. The iterated solution of this equation is,

$$\begin{aligned} \alpha \;&=\; \ln\{A/\ln\{A/\ln\{A/\cdots\}\}\} \\ &=\; \ln\{A\} - \ln\{\ln\{A\}\} + \ln\{\ln\{\ln\{A\}\}\} - \cdots \;. \end{aligned}$$

In analogy with the thin double layer, we infer that $I(A) \approx \text{constant} + \ln\{A/\ln\{A/\ln\{A/\cdots\}\}\}$. By numerical integration, it is found that to first iteration,

$$I(A) \;\approx\; \ln\{A\} + C - \;\kappa\, d \;, \quad (55)$$

where $C = -\frac{3}{4}$, while to second iteration,

$$I(A) \;\approx\; \ln\{A\} - \ln\{\ln\{A\}\} + C' \;-\; \kappa\, d \;, \quad (56)$$

where $C' = \frac{\pi}{4}$. The exact value if $I(A)$ as obtained by numerical integration is plotted in Fig.10 (the solid

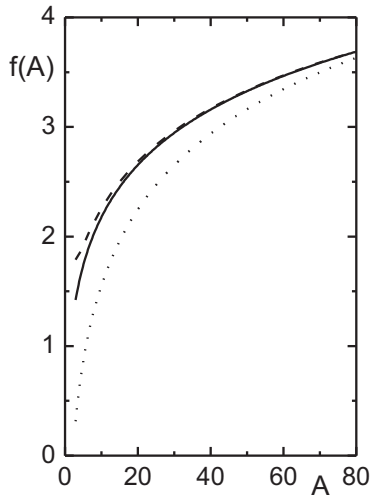

FIG. 10: The integral in eq.(54) (the solid line), the first iterated approximation (55) (the dotted line), and the second iterated approximation (56) (the dashed-dotted line). For this numerical comparison we took $\kappa d = 0$ in these plots.

line), together with the approximations (55,56) (the dotted and dashed-dotted lines, respectively). Note that the constant A for thick double layers is generally much larger than for thin double layers, since more "beads" interact simultaneously in the former case, as quantified by the prefactor $1/(\kappa\, a)^2 > 1$ in eq.(14). For the semi-quantitative description we will be satisfied with the first-order iterative approximation in eq.(55).

We thus arrive at,

$$\beta\, V_Q^{eff}(\hat{\mathbf{u}},t) \;=\; \frac{L^2}{2\,\kappa}\,\bar{\rho}\oint d\hat{\mathbf{u}}'\;\;|\,\hat{\mathbf{u}}\times\hat{\mathbf{u}}\,'|\;\;P(\hat{\mathbf{u}}\,',t) \times\int_{-1}^{1}dx\int_{-1}^{1}dx'\;\;[\,\ln\{A\}+C-\,\kappa\, d\,]\;.$$

From the definitions (22,25), with typical parameters that apply for fd-virus rods, we have $K_E/K_Q \ll 1$ up to very high degrees of condensation, so that,

$$K_Q \gg \tfrac{1}{2} K_E \mathcal{E}_0^2\;\;|\,\hat{u}_z\hat{u}_z'\,[G(\Omega x)\,G(\Omega x')+H(\Omega x)H(\Omega x')]\,|\,,$$

and we can approximate, from eq.(53),

$$\ln\{A\} \;\approx\; -\,\ln\{|\,\hat{\mathbf{u}}\times\hat{\mathbf{u}}\,'|\}+\ln\{K_Q\} - \frac{K_E}{2\,K_Q}\,\mathcal{E}_0^2\,\hat{u}_z\,\hat{u}_z'\;[\,G(\Omega x)\,G(\Omega x')+H(\Omega x)\,H(\Omega x')\,] - \tfrac{1}{2}\left[\frac{K_E}{2K_Q}\right]^2\mathcal{E}_0^4\,[\hat{u}_z\hat{u}_z']^2\,[G(\Omega x)G(\Omega x')+H(\Omega x)H(\Omega x')]^2\,. \tag{57}$$

The reason why the first *two* terms in the expansion of the logarithm are included will become clear later. The effective potential therefore consists of three distinct contributions,

$$V_Q^{eff}(\hat{\mathbf{u}},t) \;=\; \Delta V_{Q,hc}^{eff}(\hat{\mathbf{u}},t)+V_{twist}^{eff}(\hat{\mathbf{u}},t)+V_{pol}^{eff}(\hat{\mathbf{u}},t)\;,$$

where the first term is equal to,

$$\Delta V_{Q,hc}^{eff}(\hat{\mathbf{u}},t) \;=\; [\,\ln\{K_Q\}-\,\kappa\, d+C\,]\;\frac{2\,L^2}{\kappa}\,\bar{\rho} \times\oint d\hat{\mathbf{u}}'\;\;|\,\hat{\mathbf{u}}\times\hat{\mathbf{u}}\,'|\;\;P(\hat{\mathbf{u}}\,',t)\,,$$

the second contribution is given by,

$$\beta\, V_{twist}^{eff}(\hat{\mathbf{u}},t) \;=\; -\,\frac{2\,L^2}{\kappa}\,\bar{\rho} \times\oint d\hat{\mathbf{u}}'\;\;|\,\hat{\mathbf{u}}\times\hat{\mathbf{u}}\,'|\;\;\ln\{|\,\hat{\mathbf{u}}\times\hat{\mathbf{u}}\,'|\}\,P(\hat{\mathbf{u}}\,',t)\,,$$

and,

$$\beta\, V_{pol}^{eff}(\hat{\mathbf{u}},t) \;=\; -\,\frac{L^2}{4\,\kappa}\,\bar{\rho}\left[\frac{K_E}{2\,K_Q}\right]^2\mathcal{E}_0^4 \times\oint d\hat{\mathbf{u}}'\;\;|\,\hat{\mathbf{u}}\times\hat{\mathbf{u}}\,'|\;\;[\,\hat{u}_z\,\hat{u}_z'\,]^2\;P(\hat{\mathbf{u}}\,',t) \times\int_{-1}^{1}dx\int_{-1}^{1}dx'\;\;[\,G(\Omega x)\,G(\Omega x')+H(\Omega x)\,H(\Omega x')\,]^2 \tag{58}$$

Note that the term $\sim \mathcal{E}_0^2$ in eq.(57) vanishes upon integration, which is the reason that the second order term $\sim \mathcal{E}_0^4$ is included.

The potential $\Delta V_{Q,hc}^{eff}$ has the same form as the effective hard-core interaction energy (see eq.(51)). This contribution can thus be used, in the spirit of Onsager [72, 73], to define an "effective core thickness" d_{eff}. The interaction energy $V_{hc}^{eff}+\Delta V_{Q,hc}^{eff}$ can be written as a hard-core interaction potential, with a prefactor equal to $2\,d_{eff}\,L^2$ instead of $2\,d\,L^2$ as for a pure hard-core interaction potential in eq.(51), with,

$$2\,d_{eff}\,L^2 \;=\; 2\,d\,L^2+[\,\ln\{K_Q\}-\,\kappa\, d+C\,]\;\frac{2\,L^2}{\kappa}\;,$$

or,

$$\frac{d_{eff}}{d} \;=\; \frac{1}{\kappa\, d}\;[\,\ln\{K_Q\}+C\,]\;.$$

This is a semi-quantitative extension to thick double layers of Onsager's expression for the effective diameter for thin double layers [72, 73].

An asymptotic expression for the effective diameter for line charges (representing worm-like micelles) can be found in Ref.[76]. The effective diameter is also found to scale like the Debye length, with a quite similar prefactor that scales with the logarithm of the charge of the rod (see eqs.(11,34) in Ref.[76]).

The potential V_{twist}^{eff} describes the "twist effect" [74, 75]. This potential is expanded with the neglect of

fourth order terms in the orientational order parameter, by means of the Legendre polynomial expansion, with $x = \hat{\mathbf{u}} \cdot \hat{\mathbf{u}}'$,

$$|\,\hat{\mathbf{u}} \times \hat{\mathbf{u}}'\,|\;\ln\{|\,\hat{\mathbf{u}} \times \hat{\mathbf{u}}'\,|\} \;=\; \sqrt{1-x^2}\ln\sqrt{1-x^2}$$
$$= \;\frac{\pi}{4}\,\left[\frac{1}{2} - \ln 2\right]\,P_0(x) - \frac{5\pi}{32}\,\left[\frac{5}{4} - \ln 2\right]\,P_2(x) + \cdots\;.$$

As before, the contributions "$\cdots$" are on average of fourth order in the orientational order parameter (second order with respect to $\hat{\mathbf{u}}\hat{\mathbf{u}}$ and $\hat{\mathbf{u}}'\hat{\mathbf{u}}'$), which are neglected. Hence,

$$|\,\hat{\mathbf{u}} \times \hat{\mathbf{u}}'\,|\;\ln\{|\,\hat{\mathbf{u}} \times \hat{\mathbf{u}}'\,|\} \;=$$
$$\frac{21\pi}{64}\,\left[\frac{57}{84} - \ln 2\right] - \frac{15\pi}{64}\,\left[\frac{5}{4} - \ln 2\right]\,\hat{\mathbf{u}}\hat{\mathbf{u}} : \hat{\mathbf{u}}'\hat{\mathbf{u}}'\;,$$

so that,

$$\beta\,V^{eff}_{twist}(\hat{\mathbf{u}},t) \;=\; -\frac{21\,\pi}{32}\,\left[\frac{57}{84} - \ln 2\right]\,\frac{L^2}{\kappa}\,\bar{\rho}$$
$$+\frac{15\pi}{32}\,\left[\frac{5}{4} - \ln 2\right]\,\frac{L^2}{\kappa}\,\bar{\rho}\oint d\hat{\mathbf{u}}'\;\left(\,\hat{\mathbf{u}}\hat{\mathbf{u}} : \hat{\mathbf{u}}'\hat{\mathbf{u}}'\,\right)\,P(\hat{\mathbf{u}}',t)$$
$$= \;-\frac{21\,\pi}{32}\,\left[\frac{57}{84} - \ln 2\right]\,\frac{L^2}{\kappa}\,\bar{\rho} + \frac{15\pi}{32}\,\left[\frac{5}{4} - \ln 2\right]\,\frac{L^2}{\kappa}\,\bar{\rho}\,\hat{\mathbf{u}}\hat{\mathbf{u}} : \mathbf{S}\,.$$

Finally the potential V^{eff}_{pol} describes the effective interactions as induced by the field, through polarization charges. The x- and x'-integrations in eq.(58) give rise to a factor equal to,

$$\left[\,M^2(\Omega) + N^2(\Omega) + \tfrac{1}{2}\,Q^2(\Omega)\,\right]\;,$$

where,

$$M(\Omega) \;=\; \int_{-1}^{1} dx\; G^2(\Omega\,x)\;,$$
$$N(\Omega) \;=\; \int_{-1}^{1} dx\; H^2(\Omega\,x)\;,$$
$$Q(\Omega) \;=\; 2\int_{-1}^{1} dx\; G(\Omega\,x)\,H(\Omega\,x)\;.$$

These functions are accurately approximated by,

$$M(\Omega) \;=\; \tfrac{4}{3}\,\tilde{h}(\Omega)\;,$$
$$N(\Omega) \;=\; \tfrac{6}{7}\,\Omega^4\,\tilde{h}(\Omega)\;,$$
$$Q(\Omega) \;=\; \tfrac{50}{23}\,\Omega^2\,\tilde{h}(\Omega)\;,$$

where $\tilde{h}(\Omega)$ is equal to,

$$\tilde{h}(\Omega) \;=\; \frac{1}{\Omega}\,\frac{\sin\{\Omega\} + \sinh\{\Omega\}}{\left[\,\cos\{2\,\Omega\} + \cosh\{2\,\Omega\}\,\right]^2}\;,$$

so that,

$$\beta V^{eff}_{pol}(\hat{\mathbf{u}},t) = -\,\frac{L^2}{9\kappa}\,\bar{\rho}\left[\frac{K}{K_Q}\right]^2\,\tilde{h}^2(\Omega)\,\left[1+\tfrac{4}{3}\Omega^4+\tfrac{2}{5}\Omega^8\right]\,\mathcal{E}_0^4$$
$$\times\oint d\hat{\mathbf{u}}'\;\;|\,\hat{\mathbf{u}} \times \hat{\mathbf{u}}'\,|\;\left[\,\hat{u}_z\,\hat{u}'_z\,\right]^2\;P(\hat{\mathbf{u}}',t)\;.$$

With the expansion (53), and with the neglect of terms of order λ^4, it is thus found that,

$$\beta\,V^{eff}_{pol}(\mathbf{r},\hat{\mathbf{u}}) = -\frac{7\pi}{192}\,\bar{\rho}\frac{L^2}{\kappa}\,\left[\frac{K}{K_Q}\right]^2\,\tilde{h}^2(\Omega)\,\left[1+\tfrac{4}{3}\Omega^4+\tfrac{2}{5}\Omega^8\right]\,\mathcal{E}_0^4$$
$$\times\,\left(\hat{\mathbf{E}}_0\,\hat{\mathbf{E}}_0 : \hat{\mathbf{u}}\,\hat{\mathbf{u}}\right)\,\left(\hat{\mathbf{E}}_0\,\hat{\mathbf{E}}_0 : \mathbf{S}(\mathbf{r},t)\right)\;,$$

where a small term that on average is $\sim \mathbf{S}^{(4)} \odot \mathbf{S}^{(4)}$ has been neglected.

This concludes the calculation of the instantaneous effective potentials.

Appendix C : Derivation of the equation of motion for the order parameter tensor $\mathbf{S}(t)$

For the evaluation of the equation of motion for $\mathbf{S}$, two types of integrals are encountered,

$$I^{(1)}_{ij} \;=\; M_{pq}\oint d\hat{\mathbf{u}}\;\hat{u}_i\hat{u}_j\,\hat{\mathcal{R}}_n\left[\,\rho(\mathbf{r},\hat{\mathbf{u}})\,\hat{\mathcal{R}}_n\,\hat{u}_p\hat{u}_q\,\right]\;,$$
$$I^{(2)}_{ij} \;=\; M_{pqrs}\oint d\hat{\mathbf{u}}\;\hat{u}_i\hat{u}_j\,\hat{\mathcal{R}}_n\left[\,\rho(\mathbf{r},\hat{\mathbf{u}})\,\hat{\mathcal{R}}_n\,\hat{u}_p\hat{u}_q\hat{u}_r\hat{u}_s\,\right]\;,$$

where $\hat{\mathcal{R}}_n$ is the n^{th} component of the rotation operator, M_{pq} and M_{pqrs} are arbitrary matrices, while summation over repeated indices is understood. Using Stokes's theorem in the form (with $f(\hat{\mathbf{u}})$ and $h(\hat{\mathbf{u}})$ differentiable functions of $\hat{\mathbf{u}}$),

$$\oint d\hat{\mathbf{u}}\;f(\hat{\mathbf{u}})\,\hat{\mathcal{R}}\,h(\hat{\mathbf{u}}) \;=\; -\oint d\hat{\mathbf{u}}\;h(\hat{\mathbf{u}})\,\hat{\mathcal{R}}\,f(\hat{\mathbf{u}})\;, \qquad (59)$$

and using the identity,

$$\left[\hat{\mathcal{R}}_n\hat{u}_i\hat{u}_j\right]\,\hat{\mathcal{R}}_n(\cdots) = \{\hat{u}_i\partial_j + \hat{u}_j\partial_i - 2\hat{u}_i\hat{u}_j\hat{u}_n\partial_n\}\,(\cdots)\,,$$

these two integrals are evaluated as,

$$I^{(1)}_{ij} \;=\; -s_{in}\,M_{nj} - M_{in}\,s_{nj} - s_{jn}\,M_{ni} - M_{jn}\,s_{ni}$$
$$+4\,s^{(4)}_{ijnm}\,M_{mn}\;,$$
$$I^{(2)}_{ij} \;=\; -s^{(4)}_{ikmn}\,M_{jnmk} - s^{(4)}_{iknm}\,M_{njmk} - s^{(4)}_{ikmn}\,M_{nmjk}$$
$$-s^{(4)}_{ikmn}\,M_{nmkj} - s^{(4)}_{jkmn}\,M_{inmk} - s^{(4)}_{jknm}\,M_{nimk}$$
$$-s^{(4)}_{jkmn}\,M_{nmik} - s^{(4)}_{jkmn}\,M_{nmki} + 8\,s^{(6)}_{ijklmn}\,M_{nmlk}\;.$$

Multiplying both sides of the Smoluchowski equation with $\hat{\mathbf{u}}\hat{\mathbf{u}}$ and integration, and applying these two identities, it is found that the evolution equation of $\mathbf{S}$ can be written as,

$$\frac{\partial\,\mathbf{S}}{\partial\,t} \;=\; \tilde{\mathbf{\Delta}}_{id} + \tilde{\mathbf{\Delta}}_{Q,hc} + \tilde{\mathbf{\Delta}}_{twist} + \tilde{\mathbf{\Delta}}_{pol} + \tilde{\mathbf{\Delta}}_{torque}\;,$$

where $\tilde{\mathbf{\Delta}}_{id}$ is the contribution from free diffusion, $\tilde{\mathbf{\Delta}}_{Q,hc}$ stems from hard-core interactions (with an effective hard-core diameter), $\tilde{\mathbf{\Delta}}_{twist}$ is the twist contribution, $\tilde{\mathbf{\Delta}}_{pol}$ is

the contribution from interactions between polarization charges, and $\tilde{\mathbf{\Delta}}_{torque}$ is the contribution from single particle torques. The free-diffusion contribution is equal to,

$$\tilde{\mathbf{\Delta}}_{id} \;=\; 6\,D_r\,\bar{\rho}\,\left[\,\tfrac{1}{3}\,\hat{\mathbf{I}} - \mathbf{S}\,\right]\;.$$

The effective hard-core contribution $\tilde{\mathbf{\Delta}}_{Q,hc}$ is equal to,

$$\tilde{\mathbf{\Delta}}_{Q,hc} \;=\; \frac{15\pi}{8}\,d_{eff}\,L^2\,D_r\,\bar{\rho}^2\,\Big\{\,\mathbf{S}\cdot\mathbf{S} - \mathbf{S}^{(4)} : \mathbf{S}\,\Big\}\;.$$

The twist-contribution similarly found to be equal to,

$$\tilde{\mathbf{\Delta}}_{twist} = -\frac{15\pi}{8}\left[\frac{5}{4} - \ln 2\right]\frac{L^2}{\kappa}\,D_r\,\bar{\rho}^2\,\Big\{\mathbf{S}\cdot\mathbf{S} - \mathbf{S}^{(4)} : \mathbf{S}\Big\},$$

and the polarization-charge interaction contribution is,

$$\begin{aligned}\tilde{\mathbf{\Delta}}_{pol} \;&=\; \frac{7\pi}{48}\,\frac{L^2}{\kappa}\,\bar{\rho}^2\,\left[\frac{K_E}{K_Q}\right]^2\,h(\Omega)\,\mathcal{E}_0^4\,D_r \\ &\times\Big(\mathbf{S} : \hat{\mathbf{E}}_0\hat{\mathbf{E}}_0\Big)\,\Big\{\,\hat{\mathcal{S}}\,\Big(\mathbf{S}\cdot\hat{\mathbf{E}}_0\hat{\mathbf{E}}_0\Big) - \Big(\mathbf{S}^{(4)} : \hat{\mathbf{E}}_0\hat{\mathbf{E}}_0\Big)\Big\}\;,\end{aligned}$$

where the symmetrizing operator $\hat{\mathcal{S}}$ is defined as,

$$\hat{\mathcal{S}}\,\mathbf{M} \;=\; \tfrac{1}{2}\,\left[\,\mathbf{M} + \mathbf{M}^T\,\right]\;,$$

where "T" stands for "transpose".

The contribution $\tilde{\mathbf{\Delta}}_{torque}$ from single-particle torques is evaluated as follows. Multiplying the Smoluchowski equation (28) by $\hat{\mathbf{u}}\hat{\mathbf{u}}$ and integration with respect to $\hat{\mathbf{u}}$, using Stokes's theorem in the form (59), and using that,

$$\begin{aligned}\Big(\hat{\mathbf{u}}\cdot\hat{\mathbf{E}}_0\Big)\,\Big(\hat{\mathbf{u}}\times\hat{\mathbf{E}}_0\Big)\cdot\hat{\mathcal{R}}\,(\hat{\mathbf{u}}\,\hat{\mathbf{u}}) \;&=\; \\ 2\,\hat{\mathcal{S}}\,\Big(\hat{\mathbf{u}}\,\hat{\mathbf{u}}\cdot\hat{\mathbf{E}}_0\hat{\mathbf{E}}_0\Big) &- 2\,\Big(\hat{\mathbf{u}}\cdot\hat{\mathbf{E}}_0\Big)^2\,\hat{\mathbf{u}}\,\hat{\mathbf{u}}\;.\end{aligned}$$

it is found that,

$$\begin{aligned}\tilde{\mathbf{\Delta}}_{torque} \;&=\; \frac{\pi}{4}\,\beta\,L^3\,\bar{\rho}\,\epsilon\,F_1(\Omega)\,F_3\,E_0^2\,D_r \\ &\times\Big\{\,\hat{\mathcal{S}}\,\Big(\mathbf{S}\cdot\hat{\mathbf{E}}_0\hat{\mathbf{E}}_0\Big) - \mathbf{S}^{(4)} : \hat{\mathbf{E}}_0\hat{\mathbf{E}}_0\Big\}\;.\end{aligned}$$

To obtain a closed equation of motion for $\mathbf{S}$, contributions containing $\mathbf{S}^{(4)}$ must be expressed in terms of $\mathbf{S}$. We will use the closure relation (41) for $\mathbf{S}^{(4)} : \mathbf{M}$, with $\mathbf{M}$ an arbitrary matrix.

Introducing the effective volume fraction, $\varphi_{eff} = (\pi/4)\,d_{eff}^2\,L\,\bar{\rho}$ and the frequency independent constant $\tilde{F} = F_1(\Omega)\,F_3/I(\Omega)$ (with $F_1(\Omega)$, F_3, and $I(\Omega)$ defined in eq.(9)) thus leads to the equation of motion in eqs.(43,44).

[1] S. Fraden, A.J. Hurd, R.B. Meyer, Phys. Rev. Lett., 1989, **21**, 2373.
[2] U. Dassanayake, S. Fraden, A. van Blaaderen, J. Chem. Phys., 2000, **112**, 3851.
[3] A. Yethiray, A. van Blaaderen, Nature (London), 2003, **421**, 513.
[4] A-P. Hynnine, M. Dijkstra, Phys. Rev. Lett., 2005, **94**, 138303.
[5] X. Duan, W. Luo, Int. J. Mod. Phys. B, 2001, **15**, 837.
[6] M.D. Johnson, X. Duan, B. Riley, A. Bhattacharya, W. Luo, Phys. Rev. E, 2004, **69**, 041501.
[7] K.-H. Lim, E.I. Franses, J. Coll. Int. Sci. 1986, **110**, 201.
[8] Y. Hu, J.L. Glass, A.E. Griffith, S. Fraden, J. Chem. Phys., 1994, **100**, 4674.
[9] H. Isambert, A. Ajdari, J.L. Viovy, J. Prost, Phys. Rev. Lett., 1997, **78**, 971.
[10] H. Isambert, A. Ajdari, J.L. Viovy, J. Prost, Phys. Rev. E, 1997, **56**, 5688.
[11] R. Castañeda-Priego, H.H. von Grünberg, M. Kollmann, J. Phys.: Condens. Matter, 2004, **16**, S3987.
[12] P.P. Lele, M. Mittal, E.M. Furst, Langmuir, 2008, **24**, 12842.
[13] S. Procopiu, Ann. Phys., 1924, **1**, 213.
[14] Y. Bjornstahl, Phil. Mag., 1926, **2**, 701.
[15] H. Hoffmann, U. Krämer, H. Thurn, J. Phys. Chem., 1990, **94**, 2027.
[16] J. Narayanan, E. Mendes, C. Manohar, J. Phys. Chem., 1996, **100**, 18524.
[17] U. Krämer, H. Hoffmann, Macomolecules, 1991 **24**, 256.
[18] H. Kramer, C. Graf, M. Hagenbuche, C. Johner, C. Martin, P. Schwind, R. Weber, J. Phys. II France, 1994, **4**, 1061.
[19] C.T. O'Konski, S. Krause, J. Phys. Chem. 1970, **74**, 3243.
[20] S. Holzheu, H. Hoffmann, J. Phys. Chem. B, 2002, **106**, 4412.
[21] M.E. Cates, Phys. II France, 1992, **2**, 1109.
[22] X. Schlagberger, R.R. Netz, Eur. Phys. J. E, 2008, **83**, 36003.
[23] G.S. Manning, Eur. Phys. J. E, 2009, **30**, 411.
[24] G.S. Manning, Eur. Phys. J. E, 2009, **86**, 36001.
[25] M.G.L. van den Heuvel, R. Bondesan, M. Cosentino Lagomarsino, C. Dekker, Phys. Rev. Lett., 2008, **101**, 118301.
[26] F. Mantegazza, M. Caggione, M.L. Jiménez, T. Bellini, Nature Physics, 2005, **1**, 103.
[27] M.L. Jiménez, L. Fornasari, F. Mantegazza, M.C.D. Mourad, T. Bellini, Langmuir, 2012, **28**, 251.
[28] L. Fornasari, F. Mantegazza, M.L. Jimenez, M. Buscaglia, T. Bellini, Phys. Rev. E, 2009, **79**, 060401.
[29] J.P. Singh, P.P. Lele, F. Nettesheim, N.J. Wagner, E.M. Furst, Phys. Rev. E, 2009, **79**, 050401.
[30] K. Kang, J.K.G. Dhont, Eur. Phys. Lett., 2008, **84**, 14005.
[31] K. Kang, J.K.G. Dhont, Soft Matter, 2010, **6**, 273.
[32] K. Kang, J.K.G. Dhont, Eur. Phys. J. E, 2009, **30**, 333.
[33] S. Fraden, Phase transitions in Colloidal Suspensions of Virus Particles, in *Observation, Prediction and Simula-*

tion of Phase Transitions in Complex Fluids, Eds. M. Baus, L.F. Rull, J.P. Ryckaert, Kluwer Academic Publishers, Dordrecht, 1995, vol.460, NATO-ASI-Series C, p. 113.
[34] Z. Dogic, S. Fraden, Langmuir, 2000, **16**, 7820.
[35] J. Newman, H.L. Swinney, L.A. Day, J. Mol. Biol., 1977, **116**, 593.
[36] T.A. Cross, S.J. Opella, Journal of Supramolecular Structure, 1979, **11**, 139.
[37] K.G. Valentine, D.M. Schneider, G.C. Leo, L.A. Colnago, S.J. Opella, Biophysics Journal, 1986, **49**, 36.
[38] E. Grelet, S. Fraden, Phys. Rev. Lett., 2003 **90**, 198302.
[39] Z. Dogic, S. Fraden, Phil. Trans. R. Soc. Lond. A, 2001, **359**, 997.
[40] E. Grelet, M.P. Lettinga, M. Bier, R. van Roij, P. van der Schoot, J. Phys.: Cond. Matter, 2008, **20**, 494213.
[41] K.R. Purdy, S. Fraden, Phys. Rev. E, 2004, **70**, 061703.
[42] E. Pouget, E. Grelet, M.P. Lettinga, Phys. Rev. E, 2011, **84**, 041704.
[43] M.P. Lettinga, Z. Zhang, J.K.G. Dhont, S. Messlinger, G. Gompper, 2010, **6**, 4556.
[44] S. Naderi, E. Pouget, P. Ballesta, E. Grelet, P. van der Schoot, M.P. Lettinga, Phys. Rev. Lett., 2013, **111**, 037801.
[45] K. Kang, New J. Physics, 2010, **12**, 063017.
[46] F. Tombolato, A. Ferrarini, J. Chem. Phys., 2005, **122**, 054908.
[47] F. Tombolato, A. Ferrarini, E. Grelet, Phys. Rev. Lett., 2006, **96**, 258302.
[48] Z. Zhang, E. Grelet, Soft Matter, 2013, **9**, 1015.
[49] J.K.G. Dhont, K. Kang, Eur. Phys. J. E, 2011, **34**, 40.
[50] C.T. O'Konski, J. Phys. Chem., 1960, **64**, 605.
[51] K.W. Wagner, Arch. Electrotech, 1914, **2**, 371.
[52] J. Bikerman, Trans. Faraday Soc., 1940, **35**, 154.
[53] R.W. O'Brien, J. Coll. Int. Sci., 1986, **113**, 81.
[54] S.S. Dukhin, V.N. Shilov, Adv. Coll. Int. Sci., 1980, **13**, 153.
[55] D.A. Saville, T. Bellini, V. Degiorgio, F. Mantagazza, J. Chem. Phys., 2000, **113**, 6974.
[56] E.H.B. De Lacey, L.R. White, J. Chem. Soc., Faraday Trans. 2, 1981, **77**, 2007.
[57] C.S. Mangelsdorf, L.R. White, J. Chem. Soc., Faraday Trans., 1997, **93**, 3145.
[58] S.E. Pedrosa, C. Grosse, J. Coll. Int. Sci., 1999, **219**, 37.
[59] R.J. Hill, D.A. Saville, W.B. Russel, Phys. Chem. Chem. Phys., 2003, **5**, 911.
[60] H. Zhao, H.H. Bau, J. Coll. Int. Sci., 2009, **333**, 663.
[61] J. Zhou, F. Schmid, J. Phys.: Condens. Matter, 2012, **24**, 464112.
[62] R. Schmitz, B. Dünweg, Journal of Physics: Condens. Matter, 2012, **24**, 464111.
[63] J. Zhou, R. Schmitz, B. Düweg, F. Schmid, J. Chem. Phys., 2013, **139**, 024901.
[64] C. Contraras Aburto, G. Nägele, J. Chem. Phys., 2013, **139**, 134109.
[65] C. Contraras Aburto, G. Nägele, J. Chem. Phys., 2013, **139**, 134110.
[66] G.S. Manning, J. Chem. Phys., 1993, **99**, 477.
[67] W.B. Russel, D.A. Saville, W.R. Schowalter, *Colloidal Dispersions*, Cambridge University Press, Cambridge, England, 1989.
[68] J. Lyklema, *Fundamentals of Interface and Colloid Science*, Vol.I-V, Academic Press, London, England.
[69] G.S. Manning, Eur. Phys. J. E, 2011, **34**, 39.
[70] J.K.G. Dhont, R. Klein, Coll. Pol. Sci., 1987, **265**, 289.
[71] J.K.G. Dhont, W.J. Briels, J. Chem. Phys., 2003, **118**, 1466.
[72] L. Onsager, Phys. Rev., 1942, **62**, 558.
[73] L. Onsager, Ann. N.Y. Acad. Sci., 1949, **51**, 627.
[74] A. Stroobants, H.N.W. Lekkerkerker, Th. Odijk, Macromolecules, 1986, **19**, 2232.
[75] H.N.W. Lekkerkerker, G.J. Vroege, Phil. Trans. R. Soc. Lond. A, 1993, **344**, 419.
[76] Th. Odijk, J. Chem. Phys., 1990, **93**, 5172.
[77] J.K.G. Dhont, W.J. Briels, Colloids Surf. A, 2003, **213**, 131.
[78] Z. Bradac, S. Kralj, S. Zumer, Phys. Rev. E, 2002, **65**, 021705.
[79] G.S. Manning, J. Phys. Chem. B, 2009, **113**, 2231.
[80] G.S. Manning, Ber. Bunsen-Ges. Phys. Chem. Chem. Phys., 1996, **100**, 909.
[81] G.S. Manning, J. Phys. Chem. B, 2007, **111**, 8554.
[82] K. Kang, J.K.G. Dhont, Soft Matter, 2013, **9**, 4401.
[83] K. Kang, A. Wilk, A. Patkowski, J.K.G. Dhont, J. Chem. Phys., 2007, **126**, 214501.
[84] D. Kremp, W. Ebeling, H. Krienke, R. Sändig, J. Stat. Phys., 1983, **33**, 99.
[85] M.F. Holovko, T.G. Sokolovska, Journal of Molecular Liquids, 1999, **82**, 161.
[86] A. Härtel, H. Löwen, J. Phys: Condens. Matter, 2010, **22**, 104112.
[87] R. Wittkowski, H. Löwen, Molecular Physics, 2011, **109**, 2935.
[88] S. Praetorius, A. Voigt, R.Wittkowski, H. Löwen, Phys. Rev. E, 2013, **87**, 052406.